

B_K -parameter from $N_f = 2$ twisted mass lattice QCDM. Constantinou,¹ P. Dimopoulos,² R. Frezzotti,^{3,4} K. Jansen,⁵ V. Gimenez,⁶ V. Lubicz,^{7,8} F. Mescia,⁹ H. Panagopoulos,¹ M. Papinutto,¹⁰ G. C. Rossi,^{3,4} S. Simula,⁸ A. Skouroupathis,¹ F. Stylianou,¹ and A. Vladikas⁴

(ETM Collaboration)

¹*Department of Physics, University of Cyprus, P.O. Box 20537, Nicosia CY-1678, Cyprus*²*Dipartimento di Fisica, Sapienza, Università di Roma, Piazzale A. Moro, I-00185 Rome, Italy*³*Dipartimento di Fisica, Università di Roma, “Tor Vergata” Via della Ricerca Scientifica 1, I-00133 Rome, Italy*⁴*INFN, Sezione di “Tor Vergata” c/o Dipartimento di Fisica, Università di Roma**“Tor Vergata” Via della Ricerca Scientifica 1, I-00133 Rome, Italy*⁵*DESY, Zeuthen Platanenallee 6, D-15738 Zeuthen, Germany*⁶*Departament de Física Teòrica and IFIC, Univ. de València-CSIC, Dr. Moliner 50, E-46100 València, Spain*⁷*Dipartimento di Fisica, Università di Roma, Tre Via della Vasca Navale 84, I-00146 Rome, Italy*⁸*INFN, Sezione di Roma Tre c/o Dipartimento di Fisica, Università di Roma, Tre Via della Vasca Navale 84, I-00146 Rome, Italy*⁹*Departament d'Estructura i Constituents de la Matèria, Universitat de Barcelona,**6a planta, Diagonal 647 E-08028 Barcelona, Spain*¹⁰*Laboratoire de Physique Subatomique et de Cosmologie, UJF/CNRS-IN2P3/INPG, 53 rue des Martyrs, 38026 Grenoble, France*

(Received 12 October 2010; revised manuscript received 29 November 2010; published 11 January 2011)

We present an unquenched $N_f = 2$ lattice computation of the B_K parameter which controls $K^0 - \bar{K}^0$ oscillations. A partially quenched setup is employed with two maximally twisted dynamical (sea) light Wilson quarks, and valence quarks of both the maximally twisted and the Osterwalder-Seiler variety. Suitable combinations of these two kinds of valence quarks lead to a lattice definition of the B_K parameter which is both multiplicatively renormalizable and $O(a)$ improved. Employing the nonperturbative RI-MOM scheme, in the continuum limit and at the physical value of the pion mass we get $B_K^{\text{RGI}} = 0.729 \pm 0.030$, a number well in line with the existing quenched and unquenched determinations.

DOI: 10.1103/PhysRevD.83.014505

PACS numbers: 12.38.Gc, 11.10.Gh, 11.15.Ha

I. INTRODUCTION

Strong interaction effects in neutral $K^0 - \bar{K}^0$ meson oscillations are parametrized by the so-called “bag parameter” B_K [1]. Several lattice computations of B_K based on different lattice fermion discretizations have been performed throughout the years, mostly in the quenched approximation. Attention has now shifted to unquenched estimates. See Refs. [2,3] for an updated review on the subject. A compilation of recent data is provided in Fig. 1, where renormalization group invariant (RGI) values of B_K (denoted as B_K^{RGI} in this paper) are reported. Remarkably, no significant dependence of B_K^{RGI} on the number N_f of sea quark flavors is observed.

The standard way of computing B_K with Wilson fermions yields limited accuracy due to partial control of two sources of systematic effects.

(i) First of all, the $\Delta S = 2$ four-fermion operator relevant for the B_K calculation, namely,

$$O^{\Delta S=2} = \bar{s}\gamma_\mu(1 - \gamma_5)d\bar{s}\gamma_\mu(1 - \gamma_5)d, \quad (1.1)$$

mixes under renormalization with four other operators of the same dimension, but belonging to different chiral representations [4] (the so-called “wrong chirality mixing” phenomenon). The reason behind this feature is the lack of chiral symmetry of the regularized lattice action. In other regularizations (e.g. staggered or Ginsparg-Wilson

fermions) partial or full chiral symmetry ensures that the operator (1.1) is multiplicatively renormalizable (i.e. does not mix with other operators). An important detail here is that mixing actually only affects the parity-even component of the four-fermion operator (1.1). In the following we will denote it by $O_{\text{VV}+\text{AA}}$, dropping the superscript $\Delta S = 2$ for simplicity. Its parity-odd component, similarly called

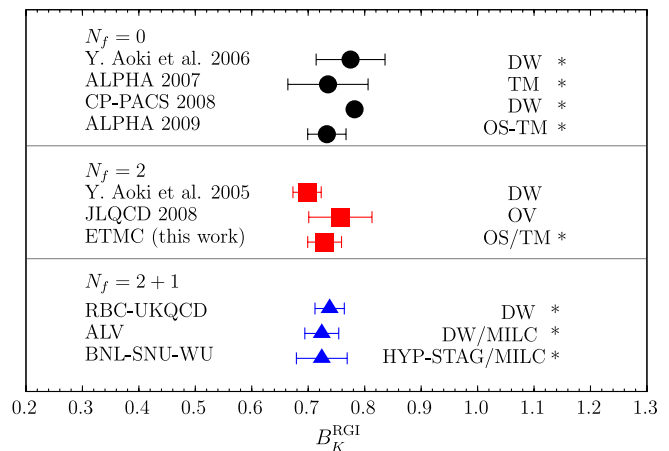


FIG. 1 (color online). A compilation of quenched and unquenched results for B_K^{RGI} . Data are from Refs. [9,15,29,42–47], respectively. The symbol “*” denotes determinations where the continuum extrapolation was carried out.

O_{VA+AV} , is protected against mixing by discrete symmetries, irrespective of the status of chiral symmetry in the lattice action, as shown in [5,6].

(ii) Second, while a lattice B_K estimate, based on staggered or Ginsparg-Wilson quarks, would be affected by only $O(a^2)$ cutoff artifacts at finite gauge coupling, computations based on plain Wilson fermions suffer from $O(a)$ discretization errors. A well-known remedy to this state of affairs is to make use of the Symanzik improvement strategy which entails the inclusion of the Clover term in the action, as well as a number of dimension-7 counterterms in the operator. However, the nonperturbative determination of the coefficients with which the counterterm operators should enter would greatly complicate the computation and increase the systematic error.

A proposal to circumvent the first of these problems was put forward in Ref. [7], where by the use of Ward-Takahashi identities (WTIs) it was shown that the matrix element $\langle \bar{K}^0 | O_{VV+AA}(0) | K^0 \rangle$ can be expressed in terms of the matrix element $\int d^4x \langle \bar{K}^0 | O_{VA+AV}(0) P(x) | K^0 \rangle$, where P is the pseudoscalar quark density. It is seen that the latter involves the multiplicatively renormalizable parity-odd part of the four-fermion operator (1.1). The price to pay for this result is that now one has to compute a four-point correlation function (while normally B_K is obtained from the large-time asymptotic limit of a three-point correlation function). This implies increased statistical fluctuations which, in practice, may offset the gain stemming from the absence of wrong chirality mixings [8].

Other attempts to avoid this problem have been tried out in Refs. [9,10], inspired by the twisted-mass formulation of lattice QCD (tm-LQCD) [11]. Two possibilities have been explored.

The first one consists in using a lattice fermion action with a maximally twisted up-down fermion doublet and a standard (untwisted) Wilson strange quark. As a second possibility, viable only in the quenched approximation (for lack of reality of the resulting fermion determinant), a degenerate down-strange doublet with twist angle $\pi/4$ is introduced. In both variants the change of variables that brings the tm-LQCD quark action to the standard Wilson form happens to map the parity-even $\Delta S = 2$ operator onto its parity-odd counterpart, thereby implying multiplicative renormalizability.

All the methods described above [7,9,10], while avoiding the operator mixing problem, lead to B_K estimates which suffer from $O(a)$ discretization effects. Achieving $O(a)$ improvement, without the use of Symanzik counterterms, necessitates having all fermions at maximal twist (Mtm-LQCD [12]). Clearly, this must be done while preserving the mapping from a parity-even to a parity-odd $\Delta S = 2$ operator, so as not to lose multiplicative renormalizability (see the discussion in Ref. [13]).

This can actually be achieved by using a different regularization for sea and valence quarks. The idea proposed in

Ref. [14] and adopted in the present study is to have maximally twisted sea quarks in combination with Osterwalder-Seiler (OS) valence quarks. We recall that any OS fermion can be thought of as a component of a maximally twisted doublet with twist angle $+\pi/2$ or $-\pi/2$, depending on the value of its Wilson r parameter.

Then the relevant $\Delta S = 2$ four-fermion operator is defined in terms of four distinct (maximally twisted) valence flavors, three with twist angle, say, $+\pi/2$, and the fourth with twist angle $-\pi/2$. The discrete symmetries of the valence quark action combined with the structure of the resulting four-fermion operator ensure that the latter is multiplicatively renormalizable, while its $K^0 - \bar{K}^0$ matrix element remains automatically $O(a)$ improved [14]. The same is then true for B_K .

In the setup of Ref. [14] unitarity violations occur as a consequence of the different regularization of sea and valence quarks. However, if renormalized masses of sea and valence fermions are matched, one can prove [14] that unitarity violations are mere $O(a^2)$ effects. Moreover, it just happens that the valence quark content of the K^0 meson consists of a strange/down pair with, say, the same twist angle, while the \bar{K}^0 meson has necessarily a quark-antiquark pair with opposite twist angles. Thus the two pseudoscalar mesons have masses that at nonzero lattice spacing differ by (numerically important) $O(a^2)$ effects, which mainly come from the lattice artifacts (non-vanishing in the chiral limit) of the K^0 -meson mass. The \bar{K}^0 -meson mass, on the other hand, exhibits only $O(a^2(\mu_\ell + \mu_s))$ discretization errors (here $\mu_{\ell/s}$ denotes the mass of the light/strange quark). This effect has been recently studied in the quenched approximation adding the clover term in Ref. [15], where it is numerically demonstrated that the scaling behavior of both B_K and the decay constants of the K^0 and \bar{K}^0 mesons is only weakly affected (see also below). The situation about the $O(a^2)$ mass splitting between K^0 and \bar{K}^0 is similar to the one already met in the unitary Mtm-LQCD framework, where a large $O(a^2)$ artefact is only observed in the mass of the neutral pseudoscalar meson as it is not associated with a conserved lattice axial current [16,17].

In this paper we present an unquenched computation of B_K based on the strategy of Ref. [14], which exploits the lattice data coming from the state-of-the-art tm-LQCD simulations carried out by the ETM Collaboration with $N_f = 2$ dynamical (sea quark) flavors, at three lattice spacings and “light” pseudoscalar meson masses in the range $280 \text{ MeV} < m_{PS} < 550 \text{ MeV}$. Renormalization is carried out nonperturbatively in the RI-MOM scheme [18]. In the continuum limit and at the physical value of the pion mass we get

$$B_K^{\text{RGI}} = 0.729(25)(17) \Leftrightarrow 0.729(30) \quad @ N_f = 2, \quad (1.2)$$

where in the first expression the two errors quoted are the statistical one (0.025) and (our estimate of) the systematic

uncertainty (0.017, resulting from the quadratic sum of 0.004 from renormalization, 0.009 from control/removal of cutoff effects, and 0.014 from extrapolation/interpolation to the physical quark mass point). In the second expression the total error is obtained by a sum in quadrature of the statistical and systematic ones. The error budget is further discussed in Sec. III B. The specification @ $N_f = 2$ is to remind us that the whole computation of B_K^{RGI} has been carried out in QCD with two light (u and d) dynamical quark flavors. The quality of this result is extremely satisfactory and fully comparable with other quenched and unquenched numbers (see Fig. 1 for a compilation of recent determinations).

The outline of the paper is as follows. In Sec. II we briefly recall the theoretical framework which allows us to obtain an $O(a)$ improved and multiplicatively renormalizable lattice expression of the $K^0 - \bar{K}^0$ matrix element of the four-fermion $\Delta S = 2$ operator (1.1). In Sec. III we give the details of our numerical analysis. Conclusions can be found in Sec. IV. We defer to a couple of appendixes a few more technical considerations. Preliminary reports about the present work have already appeared in Refs. [3,19,20].

II. TWISTED AND OSTERWALDER-SEILER VALENCE QUARKS AT MAXIMAL TWIST

The lattice setup of our study is that of Ref. [14]. The regularization of sea quarks is different from that of valence quarks. The former is a standard tm-LQCD regularization with a doublet of degenerate, maximally twisted Wilson fermions (representing up and down flavors). In the so-called ‘‘physical’’ basis, the Mtm-LQCD fermionic action takes the form

$$S_{\text{Mtm}} = a^4 \sum_x \bar{\psi}(x) \left\{ \frac{1}{2} \sum_{\mu} \gamma_{\mu} (\nabla_{\mu} + \nabla_{\mu}^*) - i\gamma_5 \tau^3 \left[M_{\text{cr}} - \frac{a}{2} \sum_{\mu} \nabla_{\mu}^* \nabla_{\mu} \right] + \mu_{\text{sea}} \right\} \psi(x), \quad (2.1)$$

where the Wilson’s r parameter has been set to unity, $\psi(x)$ is the quark flavor doublet, ∇_{μ} and ∇_{μ}^* are nearest-neighbor forward and backward lattice covariant derivatives, μ_{sea} is the (twisted) sea quark mass, and M_{cr} is the critical mass. The lattice pure gauge action is the tree-level improved action of Ref. [21], routinely adopted by the ETM Collaboration [22] in studies with two light sea quark flavors. Valence quarks are regularized as OS fermions [23]. The action of each OS valence flavor q_f reads

$$S_{\text{OS}} = a^4 \sum_x \bar{q}_f(x) \left\{ \frac{1}{2} \sum_{\mu} \gamma_{\mu} (\nabla_{\mu} + \nabla_{\mu}^*) - i\gamma_5 r_f \left[M_{\text{cr}} - \frac{a}{2} \sum_{\mu} \nabla_{\mu}^* \nabla_{\mu} \right] + \mu_f \right\} q_f(x), \quad (2.2)$$

where aM_{cr} is the same number as in Eq. (2.1). The critical mass M_{cr} is nonperturbatively tuned to its optimal value [24] as described in Ref. [22]. This ensures $O(a)$ improvement of

physical observables and control of the leading chirally enhanced cutoff effects.¹

A. Lattice operators

For the computation of interest, it is convenient to introduce four OS valence quark flavors q_1, q_2, q_3, q_4 . Eventually q_1 and q_3 will be identified with the strange quark by setting $\mu_1 = \mu_3 \equiv \mu_h$, and q_2 and q_4 with the down quark by setting $\mu_2 = \mu_4 \equiv \mu_\ell$. The key point is that the four-fermion operator

$$Q_{VV+AA} = 2\{[\bar{q}_1 \gamma_{\mu} q_2][\bar{q}_3 \gamma_{\mu} q_4] + [\bar{q}_1 \gamma_{\mu} \gamma_5 q_2] \times [\bar{q}_3 \gamma_{\mu} \gamma_5 q_4] + (q_2 \leftrightarrow q_4)\} \quad (2.3)$$

is multiplicatively renormalizable once the Wilson parameters appearing in the action of the OS fermions are taken to satisfy the relations

$$r_1 = r_2 = r_3 = -r_4. \quad (2.4)$$

The factor 2 in the right-hand side (r.h.s.) of Eq. (2.3) guarantees that the correlator (2.11), where Q_{VV+AA} is inserted between the interpolating $K^0 = \bar{q}_2 q_1$ and $\bar{K}^0 = \bar{q}_3 q_4$ fields, is normalized as in continuum QCD (as one can check by direct application of the Wick theorem). The proof of the multiplicative renormalizability of the operator Q_{VV+AA} is based on the discrete symmetries of the OS action and is provided in full detail in Ref. [14]. A simpler proof is readily obtained in the so-called ‘‘twisted basis.’’ In fact, upon performing the chiral field rotation

$$q_f \rightarrow q_f^{\text{tm}} = e^{i\pi r_f \gamma_5 / 4} q_f, \quad \bar{q}_f \rightarrow \bar{q}_f^{\text{tm}} = \bar{q}_f e^{i\pi r_f \gamma_5 / 4} \quad (2.5)$$

from the ‘‘physical’’ (q_f) to the ‘‘twisted’’ (q_f^{tm}) basis, the valence quark action in the massless limit (all μ_f ’s set to zero) takes the standard (untwisted) Wilson form, while the parity-even operator Q_{VV+AA} gets rotated onto the parity-odd Q_{VA+AV} . The latter, being expressed in terms of quark fields with standard Wilson action, is known [5,6] to be multiplicatively renormalizable. Moreover, the argument implies that the renormalized operator is given by the formula

$$[Q_{VV+AA}]_{\text{R}} = Z_{VA+AV} Q_{VV+AA}, \quad (2.6)$$

where, for consistency with the literature on Wilson fermions, the renormalization constant is named after the form (VA + AV) the operator takes in the twisted basis. In actual simulations we fixed the common value in Eq. (2.4) by setting $r_1 = 1$.

¹At the formal level a ghost action is also involved to cancel the fermionic determinant, arising from the integration over the q_f and \bar{q}_f valence degrees of freedom [14]. The presence of ghosts has no practical consequences in the evaluation of correlation functions of operators where no ghost fields appear.

In order to compute B_K , we also need to consider the axial currents

$$A_\mu^{12} = \bar{q}_1 \gamma_\mu \gamma_5 q_2, \quad A_\mu^{34} = \bar{q}_3 \gamma_\mu \gamma_5 q_4, \quad (2.7)$$

which, as a consequence of the relations between the Wilson parameters r_1, \dots, r_4 specified in Eq. (2.4), when passing from the physical to the twisted basis, take the form of axial and vector operators, respectively. Consequently, they renormalize according to the relations

$$[A_\mu^{12}]_R = Z_A A_\mu^{12}, \quad [A_\mu^{34}]_R = Z_V A_\mu^{34}. \quad (2.8)$$

B. Lattice correlation functions

Next we proceed to construct the correlation functions, involving the operators that are necessary to evaluate B_K . The lattice is taken to be of size $L^3 \cdot T$, with periodic boundary conditions on all fields and in all directions, except for quark fields in the time direction which satisfy antiperiodic boundary conditions. At a reference time slice y_0 , we define a “ K -meson wall” with pseudoscalar quantum numbers and \bar{q}_2 - and q_1 -quark fields, namely,

$$W^{21}(y_0) = \left(\frac{a}{L}\right)^3 \sum_{\vec{y}} \bar{q}_2(\vec{y}, y_0) \gamma_5 q_1(\vec{y}, y_0). \quad (2.9)$$

A second K -meson wall, $W^{43}(y_0 + T/2)$, with \bar{q}_4 - and q_3 -quark fields, is placed at the time slice $y_0 + T/2$. The four-fermion operator Q_{VV+AA} is inserted at position $x = (\vec{x}, x_0)$, with x_0 in the range $y_0 \ll x_0 \ll y_0 + T/2$. In this way, lattice estimators of the bare B_K parameter can be calculated at several values of x_0 from the ratio

$$R(x_0) = \frac{C_3(x_0)}{C_2(x_0)C'_2(x_0)} \quad (2.10)$$

involving the correlation functions²

$$C_3(x_0) = \left(\frac{a}{L}\right)^3 \sum_{\vec{x}} \left\langle W^{43}\left(y_0 + \frac{T}{2}\right) Q_{VV+AA}(x) W^{21}(y_0) \right\rangle, \quad (2.11)$$

$$C_2(x_0) = \left(\frac{a}{L}\right)^3 \sum_{\vec{x}} \langle A_0^{12}(x) W^{21}(y_0) \rangle, \quad (2.12)$$

$$C'_2(x_0) = \left(\frac{a}{L}\right)^3 \sum_{\vec{x}} \left\langle W^{43}\left(y_0 + \frac{T}{2}\right) A_0^{34}(x) \right\rangle. \quad (2.13)$$

The signal-to-noise ratio is greatly enhanced by summing over the spatial position of the quark and antiquark fields in each K -meson wall, as well as summing over that of the four-fermion operator. The x_0 behavior of the B_K

²In order to simplify the notation, we do not display the dependence on the reference time slice y_0 . The latter is chosen randomly on each gauge configuration so as to reduce the magnitude of the autocorrelation time of B_K lattice estimators.

estimator excludes significant contaminations from excited states (see also Sec. III A). On the other hand, in order to reduce the cost of computing the quark propagators, we chose to employ a stochastic method. This consists in computing quark propagators by inverting the lattice Dirac operator for the relevant OS valence quark flavors on random sources of the form

$$\delta_{\alpha\gamma} \delta_{x_0, z_0} \delta_{ik} \delta_{\vec{x}, \vec{z}} \eta^{(z_0)}(k, \vec{z}), \quad \gamma = 1, 2, 3, 4, \\ z_0 = y_0, y_0 + T/2, \quad (2.14)$$

with free indices α (spin), x_0 (time), i (color), and \vec{x} (space), while γ and z_0 are fixed as indicated. The Z_2 -valued η vectors carry only color and three-space indices (color and three-space “dilution”) and are normalized according to

$$\langle \eta^{(z_0)}(k, \vec{z}) \eta^{(z_0)}(k', \vec{z}') \rangle = \delta_{kk'} \delta_{\vec{z}\vec{z}'}. \quad (2.15)$$

Given the pattern of Wilson r parameters specified in Eq. (2.4) and the invariance under γ_5 -Hermitian conjugation combined with $r_f \rightarrow -r_f$ of the OS lattice Dirac operator, it is enough to compute for each gauge configuration the propagator of the fields q_1 and \bar{q}_2 on the random source at y_0 , and the propagator of the fields q_3 and q_4 on the random source at $y_0 + T/2$. The conditions (2.15) guarantee that unbiased estimators of the correlators C_3 , C_2 , and C'_2 are obtained.³ We found that, for an ensemble of a few hundred gauge configurations, employing one set of Z_2 -valued random sources [namely, those in Eq. (2.14)] per gauge configuration is sufficient to achieve a good statistical precision for our B_K estimators.

C. Lattice estimator of (renormalized) B_K

As we said, the masses of (up/down) sea quarks and the masses $[\mu_2]_R$, $[\mu_4]_R$ of (down) valence quarks must be tuned to the same (physical) value. At the same time, the valence mass parameters $[\mu_1]_R$ and $[\mu_3]_R$ should be adjusted to the strange quark mass in order for the external states to be identified with K particles.⁴ In this way, the renormalized ratio $\hat{R}(x_0) \equiv \frac{Z_{VA+AV}}{Z_A Z_V} R(x_0)$ computed with distinct OS valence flavors in the partially quenched setup specified above will differ from its continuum limit by only $O(a^2)$ discretization errors.

One peculiar feature of our approach which we have to keep in mind in the analysis of simulation data is the fact that kaon and antikaon masses are not degenerate, as the two mesons involve differently regularized valence quarks. In our setting the kaon is made up of the valence quarks $q_2 \rightarrow q_d$ and $q_1 \rightarrow q_s$ with $r_1 = r_2$, while the antikaon

³This setup was first presented in [19].

⁴We recall that, since the quark mass renormalization constant of OS valence quarks is independent of the sign of the corresponding Wilson r parameter [14], at the level of bare masses we must simply require $\mu = \mu_2 = \mu_4$ and $\mu_1 = \mu_3$.

consists of the valence quarks $q_4 \rightarrow q_d$ and $q_3 \rightarrow q_s$ with $r_3 = -r_4$. The $K^0 - \bar{K}^0$ mass difference $M^{12} - M^{34} \rightarrow M_K - M_{\bar{K}}$ is an $O(a^2)$ effect which has an origin similar to that of the well-known mass splitting one encounters in the pion sector [17]. Naturally the relative effect is much less important in the kaon case, as the kaon mass is substantially larger than the pion mass.⁵

Taking this mass difference into account, we write for the three-point correlation function the large-time expansion ($y_0 \ll x_0 \ll y_0 + T/2$)

$$L^6 C_3(x_0) \rightarrow \langle 0|W^{43}(0)|P^{34}\rangle \langle P^{34}|Q_{VV+AA}(0)|P^{21}\rangle \\ \times \langle P^{21}|W^{21}(0)|0\rangle \frac{1}{4M^{12}M^{34}} \exp[-M^{12}(x_0 - y_0)] \\ \times \exp\left[-M^{34}\left(y_0 + \frac{T}{2} - x_0\right)\right]. \quad (2.16)$$

In this expression $|P^{ij}\rangle$ denotes a zero three-momentum pseudoscalar state with quark content q_i and \bar{q}_j ($i, j = 1, \dots, 4$) and mass M^{ij} . Similarly we have

$$L^3 C_2(x_0) \rightarrow \langle 0|A_0^{12}(0)|P^{21}\rangle \langle P^{21}|W^{21}(0)|0\rangle \frac{1}{2M^{12}} \\ \times \exp[-M^{12}(x_0 - y_0)], \quad (2.17)$$

$$L^3 C_2'(x_0) \rightarrow \langle 0|W^{43}(0)|P^{34}\rangle \langle P^{34}|A_0^{34}(0)|0\rangle \frac{1}{2M^{34}} \\ \times \exp\left[-M^{34}\left(y_0 + \frac{T}{2} - x_0\right)\right]. \quad (2.18)$$

Furthermore, defining the pseudoscalar decay constants F^{ij} through the equations

$$\langle 0|A_0^{12}(0)|P^{21}\rangle = M^{12}F^{12}, \quad \langle P^{34}|A_0^{34}(0)|0\rangle = M^{34}F^{34}, \quad (2.19)$$

one finds that they are not equal, but again they differ by $O(a^2)$ effects.

The renormalized lattice B_K parameter which we will have to extrapolate to the continuum limit is finally obtained by averaging over the x_0 plateau (which lies between y_0 and $y_0 + T/2$) of the estimator $\hat{R}(x_0)$ viz.

$$\frac{8}{3}\hat{B}_{K,\text{lat}} \leftarrow \hat{R}(x_0) \equiv \frac{Z_{VA+AV}}{Z_A Z_V} R(x_0) \\ = \frac{Z_{VA+AV}}{Z_A Z_V} \frac{\langle P^{34}|Q_{VV+AA}(0)|P^{21}\rangle}{M^{12}F^{12}M^{34}F^{34}}, \quad (2.20)$$

where the exponentials in Eqs. (2.16), (2.17), and (2.18) exactly cancel out and the numerical factor $8/3$ in the left-hand side of this equation is there for conventional reasons; i.e. it ensures that B_K represents the four-fermion matrix

element in units of the vacuum saturation approximation value.

D. Scaling checks

In this section we present some tests aimed at checking the size of the discretization errors affecting the quantities that enter our computation of B_K [i.e. those that appear in Eq. (2.20)]. In order to keep the issue of lattice artifacts separated from those related to the extrapolation to the “physical quark mass point,” the present scaling tests have been performed at fixed reference values of the renormalized “light” and “heavy” (would-be strange) quark masses in the $\overline{\text{MS}}$ scheme at the scale of 2 GeV. For convenience, we take $\hat{\mu}_\ell^* \sim 40$ MeV and $\hat{\mu}_h^* \sim 90$ MeV.

In Fig. 2, panels (a) and (b), we show the scaling behavior of $(M^{34}/f_0)^2$ and F^{34}/f_0 , i.e. the mass squared and the decay constant of the “kaon” made up of valence quarks \bar{q}_4 and q_3 , normalized by the chiral limit pion decay constant $f_0 \simeq 121$ MeV determined in Ref. [25]. Owing to the choice $r_3 = -r_4$ the quantities M^{34} and f^{34} are our lattice estimators of the kaon mass and decay constant that should exhibit the best scaling properties. The plots in panels (a) and (b) fully confirm this expectation, showing a nice a^2 scaling with cutoff effects for the lattice kaon mass and decay constant estimates that are at the level of a few percent (from the largest lattice spacing to the continuum limit).

In Fig. 2, panels (c) and (d), we show instead the scaling behavior of the difference of the kaon mass squared and decay constant lattice estimators entering our B_K computation, namely,

$$\Delta_M = \frac{(M^{12})^2 - (M^{34})^2}{(M^{34})^2}, \quad \Delta_F = -\frac{F^{12} - F^{34}}{F^{34}}. \quad (2.21)$$

The quantities (2.21) are, by construction, mere $O(a^2)$ lattice artifacts. We see from panels (c) and (d) that both Δ_M and Δ_F extrapolate nicely to zero in the continuum limit, as expected. The large values of Δ_M in Fig. 2(c) signal the presence of a substantial cutoff effect on M^{12} , with M^{12} on the coarsest lattice differing by about 30% from its continuum limit value (~ 570 MeV). On the other hand, the lattice artifact difference between F^{12} at the largest lattice spacing and its continuum limit value is only about 5%. This is readily inferred by comparing Figs. 2(b) and 2(d).

Having taken $r_1 = r_2$, the large and positive lattice artifact observed in M^{12} was expected since for OS valence quark doublets (unlike the case of twisted-mass quark pairs), no isospin component of the lattice isotriplet axial current is conserved in the limit of vanishing quark mass. Relying on arguments similar to those given in Ref. [17], one can, however, conjecture that the large discretization error in M^{12} is due to dynamically large matrix elements entering the Symanzik description of the lattice OS pseudoscalar meson mass, rather than to large coefficients

⁵The scaling of the $K^0 - \bar{K}^0$ mass splitting has been studied in detail in the quenched approximation in Ref. [15].

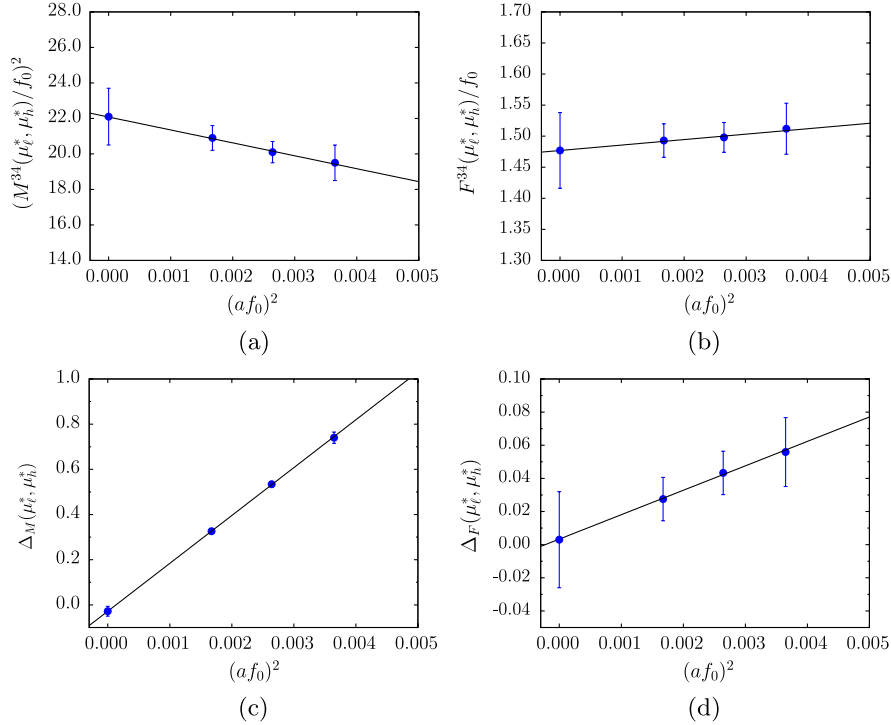


FIG. 2 (color online). Data for $(M^{34}/f_0)^2$ [panel (a)], F^{34}/f_0 [panel (b)], Δ_M [panel (c)], and Δ_F [panel (d)] as functions of $(af_0)^2$ at the reference quark masses $\hat{\mu}_\ell^* \sim 40$ MeV and $\hat{\mu}_h^* \sim 90$ MeV (in the $\overline{\text{MS}}$ scheme at 2 GeV). We display the best linear fit in $(af_0)^2$ and the corresponding continuum limit result.

in front of some terms of the Symanzik local effective action for OS valence fermions.⁶ This conjecture suggests that the large cutoff effect detected in the lattice OS pseudoscalar meson mass is peculiar to this quantity (or to others directly related to it) but not a general feature of physical observables built in terms of OS valence quarks. The small cutoff effects observed in F^{12} are well in line with such an expectation.

In Fig. 3 we show the scaling behavior of $B_{K,\text{lat}}^{\text{RGI}}(\hat{\mu}_\ell^*, \hat{\mu}_h^*)$ evaluated according to Eq. (2.20) using two different methods (referred to as M1 and M2) for the evaluation of the renormalization constants Z_{VA+AV}^{RGI} and Z_A . The two methods (discussed in Sec. III B 1 and Appendix A) differ only in the way one deals with $O(a^2)$ artifacts and other unwanted systematic effects pertaining to the RI-MOM scheme computation of renormalization constants. The somewhat different slope in a^2 of the data points in Fig. 3 should be ascribed to these effects. Nevertheless, in both cases the a^2 -scaling behavior of $B_{K,\text{lat}}^{\text{RGI}}(\hat{\mu}_\ell^*, \hat{\mu}_h^*)$ is very good and the extrapolated continuum limit values agree very well. Cutoff artifacts in $B_{K,\text{lat}}^{\text{RGI}}(\hat{\mu}_\ell^*, \hat{\mu}_h^*)$ are about 10% with method M1 and a bit larger if method M2 is adopted.

⁶When extending the analysis of Ref. [17] to the OS doublet case, one finds that, in contrast to the situation in the twisted-mass doublet case, matrix elements with both one insertion of the $d = 6$ Symanzik local effective action term and two insertions of the $d = 5$ term contribute to the cutoff effects in $(M^{12})^2$.

Two remarks are in order here. First of all, our choice of the lattice normalization factor $(M^{12}F^{12}M^{34}F^{34})^{-1}$ in the r.h.s. of Eq. (2.20) turns out to be very beneficial, as it partially compensates the discretization errors coming

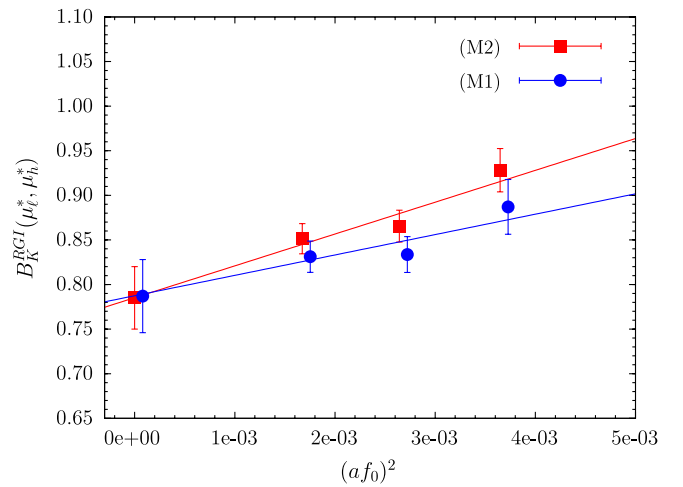


FIG. 3 (color online). $B_{K,\text{lat}}^{\text{RGI}}$ as a function of $(af_0)^2$, at the same reference quark masses, $\hat{\mu}_\ell^*$ and $\hat{\mu}_h^*$, as in Fig. 2, is shown together with the best fit linear in a^2 and the corresponding continuum limit result. The two sets of data, labeled as M1 and M2, come from different procedures for evaluating the renormalization constants Z_{AV+VA} and Z_A , expected to agree in the continuum limit.

TABLE I. Pseudoscalar masses, decay constants, and the (bare) ratio R at $\beta = 3.80$. The time plateaux “ x_0 plat.” in column 7 correspond to the interval $a^{-1}[x_0^{\min}, x_0^{\max}]$ over which the correlators C_2 and C'_2 have been taken, and in column 9 to the interval $a^{-1}[(x_0 - y_0)^{\min}, (x_0 - y_0)^{\max}]$ over which the correlator C_3 has been taken (see Sec. II B). N_{meas} denotes the number of (well-separated) gauge configurations on which the various correlators have been evaluated.

$\beta = 3.80, a \sim 0.10$ fm $L^3 \times T = 24^3 \times 48a^4$									
$a\mu_\ell$	$a\mu_h$	aM^{34}	aM^{12}	aF^{34}	aF^{12}	x_0 plat.	R	x_0 plat.	N_{meas}
0.0080	0.0165	0.2558(08)	0.3393(25)	0.0894(04)	0.0883(15)	[11,23]	0.627(4)	[11,14]	170
	0.0200	0.2731(07)	0.3532(23)	0.0913(04)	0.0895(15)		0.636(3)		
	0.0250	0.2961(07)	0.3718(21)	0.0936(04)	0.0909(15)		0.647(3)		
0.0110	0.0165	0.2712(04)	0.3508(16)	0.0924(03)	0.0900(16)	[11,23]	0.632(4)	[11,14]	180
	0.0200	0.2877(04)	0.3644(14)	0.0942(03)	0.0910(16)		0.640(4)		
	0.0250	0.3098(04)	0.3828(12)	0.0966(03)	0.0924(16)		0.651(3)		

from the matrix element $\langle P^{34} | Q_{VV+AA}(0) | P^{21} \rangle$. Second, the cutoff effects in the RI-MOM scheme computation of Z_A and Z_{VA+AV} are significantly reduced when one-loop perturbative lattice artifacts [i.e. $O(a^2 g_0^2)$ effects] are subtracted. The latter have been computed in Refs. [26,27].

In conclusion, in spite of the occurrence of a substantial $O(a^2)$ artifact in the mass of the lattice state $|P^{21}\rangle$ and the ensuing fact that the $\langle P^{34} | Q_{VV+AA}(0) | P^{21} \rangle$ matrix element is evaluated with an $O(a^2)$ four-momentum transfer, the scaling of $B_{K,\text{lat}}^{\text{RGI}}(\hat{\mu}_\ell^*, \hat{\mu}_h^*)$ with a^2 is found to be well under control, thereby allowing for a reliable continuum limit extrapolation. The same is thus expected, and found to be true (see Sec. III B 2), also upon approaching the physical quark mass point.

III. SIMULATIONS, DATA ANALYSIS, AND RESULTS

The ETM Collaboration has generated $N_f = 2$ configuration ensembles at three values of the inverse bare gauge coupling (β) and at a number of light quark masses (μ_{sea}). Several quantities entering the data analysis of this paper, such as the charged pion mass $aM_{\ell\ell}^{\text{um}}$,⁷ the low-energy constants af_0 and $a\hat{B}_0$, and the chiral limit value of a/r_0 , are derived from ETM data [22,25,28]. In this paper the symbol \hat{Q} means that the quantity Q is renormalized in the $\overline{\text{MS}}$ scheme at the 2 GeV scale. We note that, since in our analysis the continuum limit value $\hat{B}_0 = Z_P B_0$ is employed, in order to evaluate the RGI quantity $B_0 \mu_\ell = \hat{B}_0 \hat{\mu}_\ell$ one must know $\hat{\mu}_\ell = Z_P^{-1} \mu_\ell$ at the β values of interest. The necessary renormalization constants of quark bilinears, such as Z_P , Z_A , and Z_V , have been computed nonperturbatively in the RI-MOM scheme [18] as reported in Ref. [26] and converted to the $\overline{\text{MS}}$ wherever necessary.

⁷We use this notation to make it clear that this is the mass of the “charged” pion which is known to be affected by only small $O(a^2 \mu_\ell, a^4)$ lattice artifacts [16,17,24].

The calculation of the four-fermion operator renormalization constant is new and is discussed below in Sec. III B 1.

A. Extracting bare B_K estimates from lattice data

In the present computation we deal with $h\ell$ pseudoscalar mesons (“kaons”) made of two valence quarks, q_h and q_ℓ , with bare masses (μ_h, μ_ℓ) . The values of the mass parameters $(a\mu_h, a\mu_\ell)$ are chosen so as to have $\ell\ell$ pseudoscalar mesons (charged “pions” with $r_u = -r_d$) with mass in the range 280–550 MeV and $h\ell$ pseudoscalar mesons with mass in the range 450–700 MeV, depending also (see Sec. II) on whether the lattice mass $M_{34} \leftrightarrow M_{\bar{K}}$, or rather $M_{12} \leftrightarrow M_K$, is considered. The value of the light quark mass parameter $a\mu_\ell$ is common for sea and valence light (the would-be u/d) quark flavors, while the heavier quark (the would-be s) is quenched. With this choice of mass parameters we will eventually be able, as discussed in Sec. III B, to make contact with the physical K^0 and \bar{K}^0 mesons by interpolating our results in $\mu_h \rightarrow \mu_s$ and extrapolating them in the $\mu_\ell \rightarrow \mu_{u/d}$ and continuum limits.

Simulation details are gathered in Tables I, II, and III, where we report, at each gauge coupling and for all the available (μ_h, μ_ℓ) combinations, the values (in lattice units) of the measured pseudoscalar meson masses and decay constants as well as the bare B_K parameter. The latter [up to a trivial factor 8/3; see Eq. (2.20)] is denoted by R and it is obtained by averaging over a plateau in $\tau \equiv x_0 - y_0$ of the lattice estimator $R(x_0)$ given in Eq. (2.10). In the table captions we specify the plateaux intervals $[(x_0 - y_0)^{\min}/a, (x_0 - y_0)^{\max}/a]$. Indeed, the quantity $R(x_0)$ must be evaluated at large time separations. In our case this means requiring that x_0 (the time coordinate where the four-fermion operator is located) is sufficiently far away from $y_0 + T/2$ and y_0 (with $y_0, y_0 + T/2$ the time coordinates of the two K -meson walls; see Sec. II B). In this way the K^0 and \bar{K}^0 states dominate the three-point correlator $C_3(x_0)$. Actually, due to the finite T extension of the lattice, it is also necessary that the contribution to the quantum-mechanical representation of $C_3(x_0)$ from states

TABLE II. Same as in Table I but for $\beta = 3.90$.

$\beta = 3.90, a \sim 0.09 \text{ fm}$ $L^3 \times T = 24^3 \times 48a^4$									
$a\mu_\ell$	$a\mu_h$	aM^{34}	aM^{12}	aF^{34}	aF^{12}	$x_0 \text{ plat.}$	R	$x_0 \text{ plat.}$	N_{meas}
0.0040	0.0150	0.2060(05)	0.2639(11)	0.0724(03)	0.0705(09)	[11,23]	0.585(5)	[11,14]	400
	0.0220	0.2401(05)	0.2915(11)	0.0757(03)	0.0725(09)		0.608(4)		
	0.0270	0.2619(05)	0.3096(11)	0.0777(03)	0.0759(09)		0.621(4)		
0.0064	0.0150	0.2179(08)	0.2762(16)	0.0755(05)	0.0736(10)	[11,23]	0.602(7)	[11,14]	200
	0.0220	0.2506(07)	0.3028(15)	0.0785(05)	0.0759(09)		0.620(6)		
	0.0270	0.2717(07)	0.3204(14)	0.0805(04)	0.0774(09)		0.631(6)		
0.0085	0.0150	0.2283(07)	0.2849(17)	0.0773(03)	0.0755(09)	[11,23]	0.606(6)	[11,14]	200
	0.0220	0.2598(07)	0.3109(15)	0.0804(03)	0.0779(08)		0.626(5)		
	0.0270	0.2803(07)	0.3281(15)	0.0823(03)	0.0794(09)		0.637(5)		
0.0100	0.0150	0.2351(07)	0.2892(14)	0.0784(04)	0.0761(09)	[11,23]	0.606(8)	[11,14]	152
	0.0220	0.2659(07)	0.3154(12)	0.0815(04)	0.0787(08)		0.625(8)		
	0.0270	0.2860(06)	0.3328(12)	0.0834(04)	0.0802(09)		0.637(7)		
$L^3 \times T = 32^3 \times 64a^4$									
0.0040	0.0150	0.2041(04)	0.2644(15)	0.0727(03)	0.0702(11)	[11,31]	0.592(5)	[11,22]	160
	0.0220	0.2381(04)	0.2917(17)	0.0758(03)	0.0722(10)		0.615(5)		
	0.0270	0.2599(04)	0.3096(15)	0.0777(03)	0.0753(09)		0.630(5)		
0.0030	0.0150	0.1982(04)	0.2558(13)	0.0720(03)	0.0701(07)	[11,31]	0.585(4)	[11,22]	300
	0.0220	0.2329(04)	0.2838(11)	0.0750(03)	0.0720(08)		0.606(4)		
	0.0270	0.2550(04)	0.3021(11)	0.0770(03)	0.0745(08)		0.619(4)		

TABLE III. Same as in Table I but for $\beta = 4.05$.

$\beta = 4.05, a \sim 0.07 \text{ fm}$ $L^3 \times T = 32^3 \times 64a^4$									
$a\mu_\ell$	$a\mu_h$	aM^{34}	aM^{12}	aF^{34}	aF^{12}	$x_0 \text{ plat.}$	R	$x_0 \text{ plat.}$	N_{meas}
0.0030	0.0120	0.1602(08)	0.1931(18)	0.0564(03)	0.0558(07)	[14,31]	0.560(6)	[14,19]	190
	0.0150	0.1751(08)	0.2053(17)	0.0578(03)	0.0566(07)		0.575(6)		
	0.0180	0.1889(08)	0.2169(16)	0.0591(03)	0.0573(07)		0.588(6)		
0.0060	0.0120	0.1739(06)	0.2034(11)	0.0600(04)	0.0585(08)	[14,31]	0.584(7)	[14,19]	150
	0.0150	0.1877(06)	0.2153(11)	0.0613(03)	0.0596(08)		0.595(7)		
	0.0180	0.2007(06)	0.2266(11)	0.0625(03)	0.0605(08)		0.605(6)		
0.0080	0.0120	0.1840(05)	0.2127(09)	0.0615(04)	0.0604(12)	[14,31]	0.600(6)	[14,19]	220
	0.0150	0.1972(05)	0.2242(09)	0.0627(04)	0.0616(12)		0.609(5)		
	0.0180	0.2097(05)	0.2351(09)	0.0638(04)	0.0626(12)		0.618(5)		

wrapping around the world, such as that from $|\pi\pi\rangle$ or the a^2 -suppressed one from $|\pi^0\rangle$, be negligible compared to the contribution from the vacuum state. For this purpose it is important that T is large enough with respect to the inverse lattice pion mass(es).

As one can appreciate from Fig. 4, panels (a), (b), and (c), the quality of our signal for $R(x_0)$ is quite good. Wider plateaux, as well as stronger suppression of unwanted vacuum-sector states wrapping around the world, are obtained when the time extension of the lattice is increased by a factor $4/3$ going from a $24^3 \times 48$ to a $32^3 \times 64$ lattice at $\beta = 3.9$ (i.e. up to $T \sim 5.8 \text{ fm}$). This is illustrated in Fig. 4(d), where the values of $R(x_0)$ and its plateau for the larger lattice are displayed. As shown in Fig. 5, no systematic effect in the plateau value of R is visible at $\beta = 3.90$

upon comparing results from the lattices $24^3 \times 48$ and $32^3 \times 64$. Similarly, by comparing data for $C_2(x_0)$ [$C'_2(x_0)$] from the two lattices, we could also establish (see Table II) the absence of significant finite volume effects in the quantities M_{12} and F_{12} (M_{34} and F_{34}). In particular, we checked that the marginally significant finite-size effect that one can notice in aM^{34} at $\beta = 3.9$ and $a\mu_\ell = 0.0040$ has a negligible impact on our determination of B_K^{RGI} .

B. Computing B_K^{RGI} at the physical point

In order to arrive at the RGI value of B_K at the physical point, we need to go through the following steps: operator renormalization at each lattice spacing, and continuum ($a \rightarrow 0$) and chiral extrapolation ($\hat{\mu}_\ell \rightarrow \hat{\mu}_{u/d}$) with $\hat{\mu}_h$

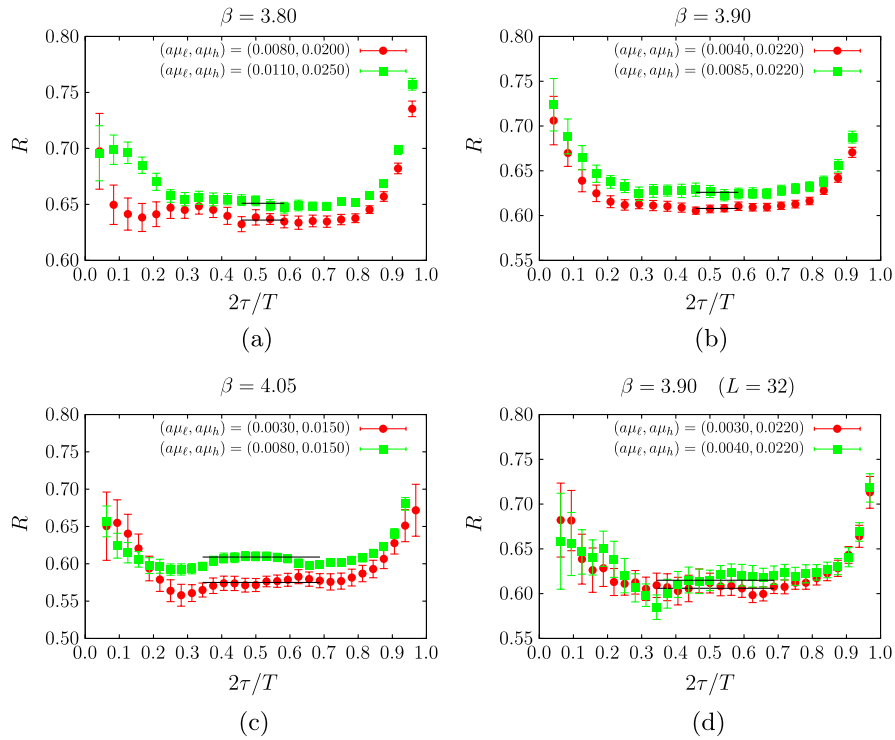


FIG. 4 (color online). Data and time plateaux for $R(x_0)$ plotted vs $2\tau/T \equiv 2(x_0 - y_0)/T$ for two different combinations of light and heavy quark masses: (a) results at $\beta = 3.80$; (b) results at $\beta = 3.90$ for the lattice $24^3 \times 48$; (c) results at $\beta = 4.05$; (d) results at $\beta = 3.90$ for the lattice $32^3 \times 64$.

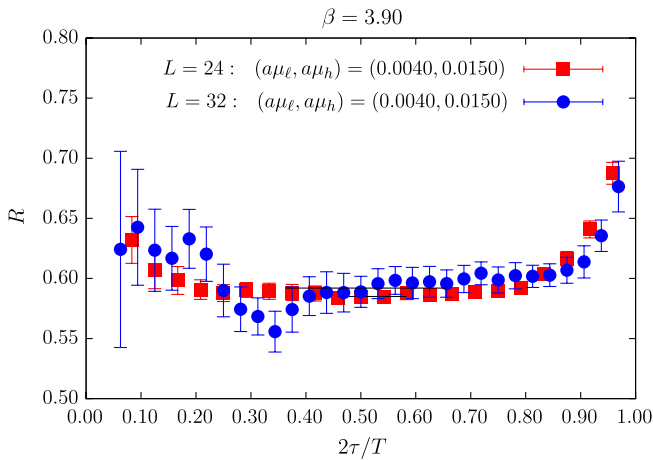


FIG. 5 (color online). Comparison of $R(x_0)$ data plotted vs $2\tau/T \equiv 2(x_0 - y_0)/T$ at two different lattice volumes for $\beta = 3.90$ and the smallest available values of μ_ℓ and μ_h .

set to the strange quark mass $\hat{\mu}_s$ as determined by using the experimental value of the kaon mass.

1. Computing Z_{AV+VA}

Renormalization of B_K requires, in particular, the calculation of the four-fermion operator renormalization constant Z_{AV+VA} in the mass-independent scheme. This task was carried out using the RI-MOM approach. We followed

the general strategy presented in Ref. [26] employing the two procedures referred to there as M1 (or extrapolation method) and M2 (or p^2 -window method). In this way, one obtains for each β two estimates of the renormalization constant at the lattice reference scale, which we will denote as $Z_{AV+VA}^{\text{RI},Mj}(a^{-2})$, $j = 1, 2$. Using the known next-to-leading order (NLO) anomalous dimension of the four-fermion operator in the RI-MOM scheme, the RGI quantities $Z_{AV+VA}^{\text{RGI},Mj}$ are evaluated. We note that the cutoff effects on the lattice estimators of Z_{AV+VA} are significantly reduced by subtracting their one-loop perturbative expression up to $O(a^2 g_0^2)$, computed in [27]. Further information on the computation of the four-fermion operator renormalization constant, including a numerical check on the absence of wrong chirality mixing, is given in Appendix A.

In the following, we will quote results obtained by employing the estimates of Z_A and Z_{AV+VA}^{RGI} from procedure M2, as well as the very precise determination of Z_V obtained in Ref. [26]. The latter is determined by comparing (matrix elements of) the local current to the exactly conserved one. We immediately notice that upon using procedure M1 for the evaluation of Z_A and Z_{AV+VA}^{RGI} , very similar results for B_K^{RGI} are obtained, with differences typically as small as 0.002 (that we include in the systematic error).⁸

⁸The consistency of the continuum limit results for the unphysical quantity $B_K^{\text{RGI}}(\hat{\mu}_\ell^*, \hat{\mu}_h^*)$ evaluated with renormalization constants from procedure M1 or M2 was noted in Sec. IID.

TABLE IV. Results for Z_{VA+AV}^{RGI} (M1, M2) from the analysis discussed in this appendix, together with the (best) final estimates of Z_A (M1, M2) and Z_V from Ref. [26], for the three β values of interest here.

β	Z_{VA+AV}^{RGI} (M1)	Z_{VA+AV}^{RGI} (M2)	Z_A (M1)	Z_A (M2)	Z_V
3.8	0.605(18)	0.620(13)	0.746(11)	0.727(07)	0.5816(02)
3.9	0.623(11)	0.630(08)	0.746(06)	0.730(03)	0.6103(03)
4.05	0.691(11)	0.698(08)	0.772(06)	0.758(04)	0.6451(03)

The values of the renormalization constants entering the present computation of B_K^{RGI} can be found in Table IV.

2. Continuum and chiral extrapolations

Continuum and chiral ($\mu_\ell \rightarrow \mu_{u/d}$) extrapolations are carried out simultaneously, exploiting the SU(2)- χ PT-based fit ansatz of Ref. [30] which, for our computation with $\mu_{\text{sea}} = \mu_\ell$, reads⁹

$$B_{K,\text{lat}}^{\text{RGI}}(\hat{\mu}_\ell, \hat{\mu}_s) = B_{K,\chi}^{\text{RGI}}(\hat{\mu}_s) \left[1 + b(\hat{\mu}_s) \frac{2\hat{B}_0 \hat{\mu}_\ell}{f_0^2} - \frac{2\hat{B}_0 \hat{\mu}_\ell}{32\pi^2 f_0^2} \times \log \frac{2\hat{B}_0 \hat{\mu}_\ell}{16\pi^2 f_0^2} \right] + a^2 f_0^2 D_B(\hat{\mu}_s), \quad (3.1)$$

where $B_{K,\text{lat}}^{\text{RGI}}(\hat{\mu}_\ell, \hat{\mu}_s)$ denotes the RGI lattice estimates of the ‘‘bag parameter’’ at renormalized ℓ -quark mass $\hat{\mu}_\ell$ and strange quark mass $\hat{\mu}_s$. Note that all dimensionful quantities are expressed in units of f_0 . The dimensionless fit parameters $B_{K,\chi}^{\text{RGI}}(\hat{\mu}_s)$, $b(\hat{\mu}_s)$, and $D_B(\hat{\mu}_s)$ are functions of $\hat{\mu}_s$. The first of them represents the RGI bag parameter at $\hat{\mu}_s$ in the SU(2)- χ PT limit ($\hat{\mu}_\ell \rightarrow 0$).

Several comments are in order here. First, as shortly mentioned above, the renormalized (in $\overline{\text{MS}}$ at 2 GeV) quantities \hat{B}_0 and $\hat{\mu}_{u/d}$ and the chiral limit pion decay constant f_0 ,

$$\hat{B}_0 = 2.84(11) \text{ GeV}, \quad \hat{\mu}_{u/d} = 3.5(1) \text{ MeV}, \\ f_0 = 121.0(1) \text{ MeV}, \quad (3.2)$$

as well as estimates of a at $\beta = 3.8, 3.9, 4.05$,

$$af_0|_{\beta=3.8} = 0.0604(16), \quad af_0|_{\beta=3.9} = 0.0514(08), \\ af_0|_{\beta=4.05} = 0.0409(07), \quad (3.3)$$

are obtained by an analysis of the data for the mass and the decay constant of the $\ell\ell$ (charged) pseudoscalar meson along the lines of Ref. [25] and using the results on the quark mass renormalization constant $Z_\mu = Z_P^{-1}$ from [26]. Here we just recall that in this analysis based on SU(2)- χ PT at NLO, we set the physical scale using the experimental value of f_π and take into account finite-size

⁹With respect to the formulas of Ref. [30], we replace Λ_χ with $4\pi f_0$ and reabsorb the effect of this change in a redefinition of $b(\hat{\mu}_h)$. We use $f_0 \simeq 121$ MeV as found in [25].

effects and $O(a^2)$ artifacts. As we rely on NLO SU(2)- χ PT formulas, the $\ell\ell$ pseudoscalar meson data are taken only from a $\hat{\mu}_\ell$ region (see Tables I, II, and III), where the impact of possible next-to-next-to-leading order (NNLO) corrections has been checked (via the methods of Ref. [25]) to be negligible.

The renormalized strange quark mass $\hat{\mu}_s$ is extracted by analyzing our data on the $h\ell$ pseudoscalar meson mass M_{34} at $\beta = 4.05, 3.9$, and 3.8 with the help of the SU(2)- χ PT-based ansatz [30],

$$f_0^{-2} M_{34}^2(\hat{\mu}_\ell, \hat{\mu}_h) = C_M(\hat{\mu}_h) \left[1 + c(\hat{\mu}_h) \frac{2\hat{B}_0 \hat{\mu}_\ell}{f_0^2} \right] + a^2 f_0^2 D_M(\hat{\mu}_h), \quad (3.4)$$

for three reference values of $\hat{\mu}_h$ in the strange quark mass region (from 75 to 105 MeV). In the fit ansatz (3.4), with all dimensionful quantities expressed in units of f_0 , we have included a term, with coefficient $D_M(\hat{\mu}_h)$, to parametrize the leading $O(a^2)$ artifacts. Finite-size effects on the raw lattice data for M_{34}^2 , although not shown in Eq. (3.4), were taken into account in our actual fits. These effects, which are checked at $\beta = 3.9$, $a\mu_\ell = 0.0040$ to be $\leq 1\%$ and only marginally significant within errors (see Table II), have been estimated by using resummed χ -PT formulas [31] and subtracted out from the lattice data. The coefficients $C_M(\hat{\mu}_h)$ and $D_M(\hat{\mu}_h)$ grow almost linearly with $\hat{\mu}_h$ in the aforementioned range, in line with the chiral behavior expected at finite lattice spacing, namely, $M_{34}^2 \sim (\hat{\mu}_\ell + \hat{\mu}_h)$ as $(\hat{\mu}_\ell + \hat{\mu}_h) \rightarrow 0$ [24].

Since at this stage the value of $\hat{\mu}_{u/d}$ is already known, once the parameters $C_M(\hat{\mu}_h)$, $c(\hat{\mu}_h)$, and $D_M(\hat{\mu}_h)$ have been determined by the fit of the $\hat{\mu}_\ell$ dependence based on Eq. (3.4), one immediately yields continuum limit estimates of $M_{34}^2(\hat{\mu}_{u/d}, \hat{\mu}_h)$ for the three chosen reference values of $\hat{\mu}_h$. These estimates exhibit a smooth dependence on $\hat{\mu}_h$ and can be interpolated linearly to the experimental value of $M_K^2 = (495 \text{ MeV})^2$, thereby providing a well-controlled result for $\hat{\mu}_s$, for which we find

$$\hat{\mu}_s \equiv \mu_s^{\overline{\text{MS}}, 2 \text{ GeV}} = 92(5) \text{ MeV}. \quad (3.5)$$

More details on this analysis will be given in a forthcoming publication [32].

Also, our lattice estimators for $B_{K,\text{lat}}^{\text{RGI}}(\hat{\mu}_\ell, \hat{\mu}_h)$ turn out to have a weak dependence on $\hat{\mu}_h$. It is thus straightforward to obtain, by linear interpolation in $\hat{\mu}_h$, their values at the

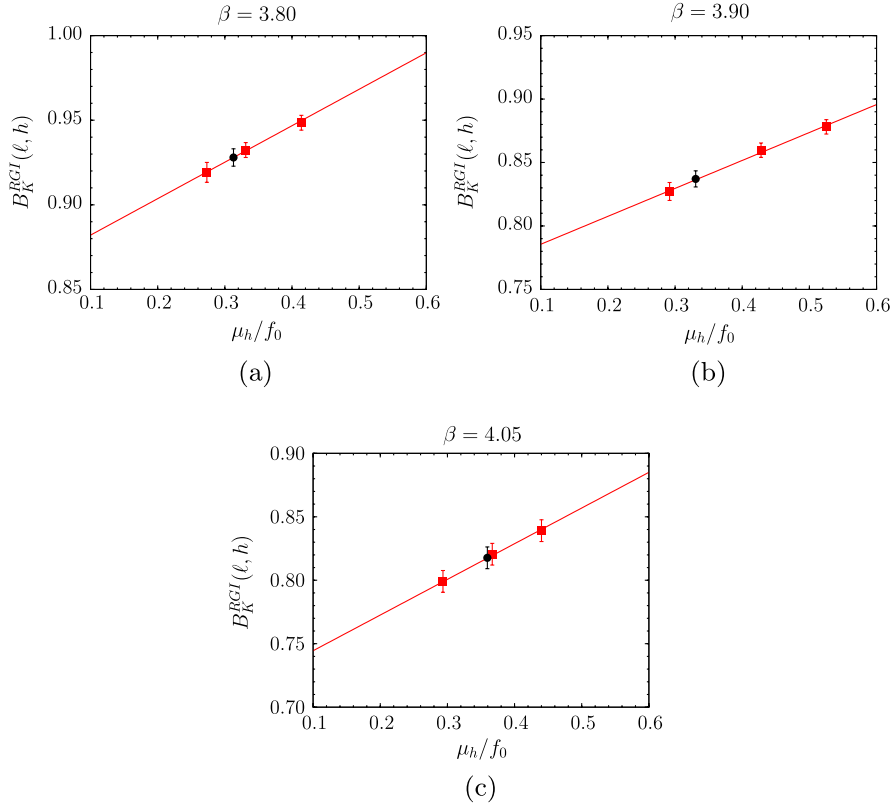


FIG. 6 (color online). Linear interpolation of $B_K^{\text{RGI}}(\hat{\mu}_\ell, \hat{\mu}_h)$ to the physical strange quark mass point $\hat{\mu}_h \rightarrow \hat{\mu}_s = 92$ MeV at ($\beta = 3.8, a\mu_\ell = 0.0080$) [panel (a)], ($\beta = 3.9, a\mu_\ell = 0.0040$) [panel (b)], and ($\beta = 4.05, a\mu_\ell = 0.0030$) [panel (c)].

point $\hat{\mu}_h = \hat{\mu}_s$. By exploiting the available determinations of $a(\beta)$ in physical units from the analysis of the pion sector data, the interpolation of $B_{K,\text{lat}}^{\text{RGI}}(\hat{\mu}_\ell, \hat{\mu}_h)$ to the s -quark mass point can be performed separately at each value of β and $a\hat{\mu}_\ell$. An example of such interpolations is shown in Fig. 6. In this way, we obtain the quantity $B_{K,\text{lat}}^{\text{RGI}}(\hat{\mu}_\ell, \hat{\mu}_s)$ for the three lattice spacings and the $a\hat{\mu}_\ell$ values corresponding to the bare parameters in Tables I, II, and III. This set of numbers can be fit to the formula (3.1), where the quantities $B_{K,\chi}^{\text{RGI}}(\hat{\mu}_s)$, $b(\hat{\mu}_s)$, and $D_B(\hat{\mu}_s)$ are the free parameters to be determined. As it clearly appears from Fig. 7, the quality of the resulting fit is very good.

3. Final result and error budget

The value of B_K^{RGI} at the physical point is finally determined by evaluating Eq. (3.1) in the continuum limit at the best-fit values of $B_{K,\chi}^{\text{RGI}}(\hat{\mu}_s)$ and $b(\hat{\mu}_s)$ and setting $\mu_\ell = \mu_{u/d}$. In this way, we arrive at the result

$$B_K^{\text{RGI}} = 0.729(25). \quad (3.6)$$

The error quoted in parentheses in Eq. (3.6) is of statistical origin. It comes from our fitting procedure and reflects the statistical errors on the raw data for the bare matrix elements and the associated renormalization constants. Its estimate has been performed via a standard bootstrap analysis, thereby taking properly into account all possible

cross correlations. As one checks in Tables I, II, and III, at fixed quark masses and lattice spacing, the typical statistical error on the bare lattice estimator of B_K is around 1%. Inspection of Table IV shows that the relative error coming from the B_K -renormalization factor $Z_{VA+AV}^{\text{RGI}}/(Z_A Z_V)$ is about 2.0%. The extrapolation to the continuum limit and

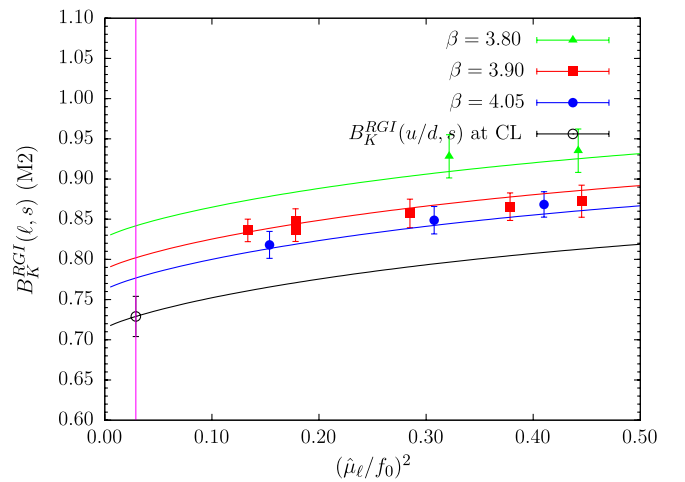


FIG. 7 (color online). Combined chiral and continuum fits according to the ansatz (3.1). The label M2 refers to the specific RI-MOM procedure adopted for the computation of Z_{VA+AV}^{RGI} and Z_A .

the physical pion mass, plus interpolation to the kaon point, finally leads to the error quoted in Eq. (3.6).

In order to try to have an idea of the size of the systematic error, other analyses have been performed besides the one discussed above.

(i) First of all, the whole analysis was repeated on the same set of raw data but choosing a/r_0 extrapolated to the chiral limit [25] (with r_0 the Sommer scale), instead of af_0 , as the scaling variable used to build dimensionless quantities suited for continuum extrapolation. This change turned out to produce an increase of the value of B_K^{RGI} of a few permille.

(ii) Second, we replaced $2\hat{B}_0\hat{\mu}_\ell$ by the squared $\ell\ell$ -meson mass $(M_{\ell\ell}^{\text{tm}})^2$ in extrapolating to the physical pion mass point, and we determined the kaon point by interpolating the quantity $(M_{hh}^{\text{tm}})^2$ to the physical value of $2M_K^2 - M_\pi^2$. As before, B_K^{RGI} increases by a few permille. Moreover, we have tried a fit function which also includes higher order analytical terms added to the SU(2)- χ PT formula. We observe a shift equal to 0.007 in the central value of B_K^{RGI} .

(iii) We also tried to perform the extrapolation to the physical pion mass point using a first or second order polynomial in μ_ℓ as an alternative to the SU(2)- χ PT-based ansatz (3.1). We obtained good quality fits, where the central value of B_K^{RGI} gets shifted by +0.021 or +0.001, respectively. Completely analogous results are obtained by employing a first or second order polynomial in $(M_{\ell\ell}^{\text{tm}})^2$.

(iv) Finally, all these alternative analyses were repeated by using the M1 method for the RI-MOM renormalization in place of M2. In all cases this produced tiny changes of B_K^{RGI} (never larger than ± 0.004). For instance, for the main analysis discussed in some detail in the present section, a decrease of B_K^{RGI} by 0.002 was observed. Further information on the analyses for the estimate of the systematic error is given in Appendix B.

In this way, we arrive at the systematic error budget for B_K^{RGI} we anticipated in the Introduction, which is detailed below. We get

- (i) 0.004 from the RI-MOM renormalization, evaluated by combining the uncertainty due to the spread coming from methods M1 and M2 and the estimated error due to the truncation to NLO of the perturbative series in the conversion from the RI-MOM scheme to RGI.
- (ii) 0.009 from the uncertainty in controlling/removing cutoff effects. In this figure we combine the neglected $O(a^4)$ lattice artifacts, which we estimate to be $\sim 1\%$,¹⁰ and the effect related to the choice of the scaling variable used in the analysis (af_0 or a/r_0).

¹⁰The estimate of $\sim 1\%$ as the natural size of the $O(a^4)$ corrections follows from the fact that we observe in our B_K^{RGI} lattice estimators $O(a^2)$ cutoff effects at a level of $\sim 10\%$.

- (iii) 0.014 from the systematic uncertainty in the extrapolation to the pion mass point, where we add in quadrature 0.004 from varying the choice of the extrapolation variable [μ_ℓ or $(M_{\ell\ell}^{\text{tm}})^2$], 0.011 from the difference between an SU(2)- χ PT-based fit and a simple polynomial ansatz (we take the average of the spread resulting from the polynomial fits discussed above), and a shift equal to 0.007 due to a possible inclusion of higher order analytical terms in the SU(2)- χ PT fit formula.

Summing in quadrature all these small systematic uncertainties leads to a total systematic error estimate of ± 0.017 . This number was added in quadrature to the statistical error in Eq. (3.6), yielding the final result quoted in Eq. (1.2).

IV. CONCLUSIONS

In this paper we have computed from the $N_f = 2$ tm-LQCD simulation data produced by the ETM Collaboration the value of the strong interaction parameter, \hat{B}_K , which controls the $K^0 - \bar{K}^0$ oscillations. To this end, we have exploited the partially quenched setup proposed in Ref. [14] which, at the price of introducing $O(a^2)$ unitarity violations, ensures $O(a)$ improvement and the absence of wrong chirality mixing effects [4]. Renormalization is carried out nonperturbatively in the RI-MOM scheme [18,26].

Using data at three lattice spacings and a number of pseudoscalar masses in the interval $280 \text{ MeV} < m_{\text{PS}} < 550 \text{ MeV}$, we get in the continuum limit of $N_f = 2$ QCD and at the physical value of the pion and kaon mass, the value of the RGI bag parameter reported in Eq. (1.2), namely, $B_K^{\text{RGI}} = 0.729 \pm 0.030$.

Our determination is quite accurate, with a $\sim 4\%$ total error (with statistical and total systematic errors added in quadrature), and agrees rather well with other existing values. In particular, from the comparison of our result for B_K with the results from $N_f = 2 + 1$ dynamical simulations (see Fig. 1), it may be inferred that the quenching of the strange quark leads to an error which is rather small, i.e. smaller, at present, than other systematic uncertainties affecting current B_K estimates. If taken at face value, our result confirms the tension between the lattice determination (which does not seem to depend significantly on the number of dynamical quark flavors) and the preferred value of recent phenomenological, standard model-based analyses (see Refs. [3,33–36]). However, some theoretical concerns remain about the way to estimate the long-distance contributions in the relation between the strong interaction parameter \hat{B}_K and the experimentally well-measured quantity ϵ_K that parametrizes the (indirect) CP violation in the $K^0 - \bar{K}^0$ system.

In order to get a substantially more accurate determination of B_K^{RGI} , we would need to increase the statistics and work at even finer lattice spacings, with the u/d -quark

mass closer to the physical point. A further, possibly important improvement is the use of data from more realistic simulations, where dynamical strange and charm sea quarks are included. Actually, the ETM Collaboration is already moving ahead in these directions [37], and work aiming at more precise lattice determinations of the kaon bag parameter is in progress.

ACKNOWLEDGMENTS

We wish to thank all the other members of ETM Collaboration for their interest in this work and a most enjoyable and fruitful collaboration. This work was supported by the European Union Sixth Framework Programme under Contract No. MTRN-CT-2006-035482, FlaviaNet. V.G. thanks the MICINN (Spain) for partial support under Grant No. FPA2008-03373 and the Generalitat Valenciana (Spain) for partial support under Grant No. GVPROMETEO2009-128. F.M. acknowledges financial support from Projects No. FPA2007-66665, No. 2009SGR502, and from the Spanish Consolider-Ingenio 2010 Programme CPAN (CSD2007-00042). M.P. acknowledges financial support by a Marie Curie European Reintegration Grant of the 7th European Community Framework Programme under Contract No. PERG05-GA-2009-249309. A. S. acknowledges financial support from the Research Promotion Foundation of Cyprus (Proposal No. ENIΣX/0506/17).

APPENDIX A: THE RI-MOM COMPUTATION OF Z_{VA+AV}

Here we discuss the nonperturbative computation of the renormalization constant (RC) of the operator Q_{VV+AA} [see Eq. (2.3)], which, for the reasons explained in Sec. II A, we call Z_{VA+AV} . It is first evaluated in the RI'-MOM scheme,¹¹ at some appropriate scale μ_0 lying in the domain of applicability of (RG-improved) perturbation theory, following the strategy detailed in Ref. [26]. Then $Z_{VA+AV}^{\text{RI}'}$ is converted into the (scheme- and scale-independent) quantity Z_{VA+AV}^{RGI} according to the formula

$$Z_{VA+AV}^{\text{RGI}} = (\alpha(\mu_0))^{-(\gamma_0/2\beta_0)} \exp\left\{\int_0^{\alpha(\mu_0)} d\alpha' \left[\frac{\gamma_{VA+AV}(\alpha')}{\beta(\alpha')} + \frac{\gamma_0}{2\beta_0\alpha'}\right]\right\} Z_{VA+AV}^{\text{RI}'(\mu_0^2)}, \quad (\text{A1})$$

where

¹¹The prime in the label RI' is to remind us about the specific defining condition adopted for the quark field RC Z_q , which, as convenient in lattice studies, is taken here to coincide with the quark propagator form factor Σ_1 . For the latter we adopt the definition of Eq. (33) of Ref. [26].

$$\beta(\alpha) = -\frac{2\beta_0}{4\pi}\alpha^2 + \mathcal{O}(\alpha^3), \quad \beta_0 = 11 - \frac{2N_f}{3},$$

$$\gamma_{VA+AV}(\alpha) = \frac{\gamma_0}{4\pi}\alpha + \mathcal{O}(\alpha^2), \quad \gamma_0 = 4, \quad (\text{A2})$$

which is evaluated here with $N_f = 2$ and to NLO accuracy [38,39]. RGI quantities are normalized following the conventions of Ref. [1]. In this appendix we quote results for Z_{VA+AV}^{RGI} but, since the conversion from RI'-MOM to RGI is a straightforward step, most of our discussion will actually concern the evaluation of $Z_{VA+AV}^{\text{RI}'(\mu_0^2)}$ at the three lattice spacings of interest for the present work. The error on B_K^{RGI} associated with the NLO perturbative conversion from RI'-MOM to RGI is estimated to be about 0.002 and has been taken into account in the error budget discussion of Sec. III B 3. This estimate is obtained assuming that the neglected NNLO and higher order relative corrections to the conversion factor are as large as the square of the NLO relative correction, which turns out to be $\simeq 5\%$.

For the purpose of determining $Z_{VA+AV}^{\text{RI}'}$, besides the q_f -quark propagator¹²

$$S_{q_f}(p) = a^4 \sum_x e^{-ipx} \langle q_f(x) \bar{q}_f(0) \rangle, \quad (\text{A3})$$

we compute the relevant Green function as the momentum space correlator

$$G_{VV+AA}(p, p, p, p)_{\alpha\beta\gamma\delta}^{abcd} = a^{16} \sum_{x_1, x_2, x_3, x_4} e^{-ip(x_1 - x_2 + x_3 - x_4)} \langle [q_1(x_1)]_{\alpha}^a \times [\bar{q}_2(x_2)]_{\beta}^b Q_{VV+AA}(0) [q_3(x_3)]_{\gamma}^c [\bar{q}_4(x_4)]_{\delta}^d \rangle. \quad (\text{A4})$$

The lowercase Greek (Latin) symbols denote uncontracted spin (color) indices. In terms of the corresponding amputated Green function¹³

$$\Lambda_{VV+AA}(p, p, p, p; \mu_{\text{val}}, \mu_{\text{sea}})_{\alpha\beta\gamma\delta}^{abcd} = [S_{q,1}(p)^{-1}]_{\alpha\alpha'}^{aa'} \times [S_{q,3}(p)^{-1}]_{\gamma\gamma'}^{cc'} G_{VV+AA}(p, p, p, p)_{\alpha'\beta'\gamma'\delta'}^{a'b'c'd'} \times [S_{q,2}(p)^{-1}]_{\beta'\beta}^{b'b} [S_{q,4}(p)^{-1}]_{\delta'\delta}^{d'd}, \quad (\text{A5})$$

the RI'-MOM RC is obtained by imposing in the chiral limit ($\mu_{\text{val}} = \mu_{\text{sea}} = 0$) the renormalization condition

$$[Z_{VA+AV}^{\text{RI}'} Z_q^{-2} D_{11}^{\text{lat}}](p; \mu_{\text{val}}, \mu_{\text{sea}}) = 1, \quad (\text{A6})$$

where Z_q denotes the (flavor-independent) quark field RC and the $VV + AA$ vertex D_{11}^{lat} is given by

¹²The equations below are written in the so-called physical quark basis with the lattice valence quark action given by Eq. (2.2).

¹³We explicitly display in the left-hand side of the equation the dependence on quark mass parameters that is implicit in the quantities appearing in the r.h.s.

$$D_{11}(p; \mu_{\text{val}}, \mu_{\text{sea}}) = \Lambda_{VV+AA}(p, p, p, p; \mu_{\text{val}}, \mu_{\text{sea}})_{\alpha\beta\alpha'\beta'}^{aabb} \mathcal{P}_{\alpha\beta\alpha'\beta'}^{VV+AA}, \quad (\text{A7})$$

where $\mathcal{P}_{\alpha\beta\alpha'\beta'}^{VV+AA}$ is a suitably normalized spin projector reflecting the $VV + AA$ Dirac structure of the vertex. Details on this projector and the notation can be found in [6].

As usual in lattice RI-MOM computations, the relevant Green functions (A3) and (A4) are evaluated in the Landau gauge for a sequence of sea $\{\mu_{\text{sea}}\}$ and valence $\{\mu_{\text{val}}\}$ -quark mass parameters at each of the three lattice spacings we consider here. The bare parameters and the statistics of this computation are detailed in Table 2 of Ref. [26]. Also, the lattice momenta p_ν , with $p_{1,2,3} = (2\pi/L)n_{1,2,3}$, $p_4 = (2\pi/L)(n_4 + 1/2)$, that we consider here are specified in Eqs. (20)–(21) of Ref. [26]. To minimize the contributions of Lorentz-noninvariant discretization effects, we have considered in our analysis only the momenta p satisfying the constraint

$$\sum_\rho \tilde{p}_\rho^4 < 0.28 \left(\sum_\nu \tilde{p}_\nu^2 \right)^2, \quad a\tilde{p}_\nu \equiv \sin(ap_\nu). \quad (\text{A8})$$

In the following, we shall often use the quantity $\tilde{p}^2 = \sum_\nu \tilde{p}_\nu^2$.

1. Sketch of procedure for extracting Z_{VA+AV}^{RGI}

Here we summarize the rather standard procedure we follow to extract Z_{VA+AV}^{RGI} , deferring the discussion of further details to subsequent subsections. First of all, for each β and each choice of the scale \tilde{p}^2 , the condition (A6) is enforced at all the values of μ_{sea} and μ_{val} given in Table 2 of Ref. [26]. By doing so, one obtains lattice approximants at nonzero quark mass(es) of the desired RC, $Z_{VA+AV}^{\text{RI}}(\tilde{p}^2; a^2\tilde{p}^2; \mu_{\text{val}}, \mu_{\text{sea}})$, which are then extrapolated to $\mu_{\text{val}} = \mu_{\text{sea}} = 0$.¹⁴

Improved and controlled estimates of $Z_{VA+AV}^{\text{RI}} \times (\tilde{p}^2; a^2\tilde{p}^2; 0, 0)$ are obtained by removing the perturbatively leading cutoff effects. Using NLO continuum QCD evolution [38,39], the first argument is brought to a reference scale value, μ_0^2 . The reliability of this step rests on the usual assumption that the scales \tilde{p}^2 and μ_0^2 are large enough to make NLO-PT accurate (within statistical errors). The remaining $a^2\tilde{p}^2$ dependence in $Z_{VA+AV}^{\text{RI}}(\mu_0^2; a^2\tilde{p}^2; 0, 0)$ is to be regarded as a mere lattice artifact which will be taken care of by employing either the M1 or M2 method (introduced in Ref. [26]), as briefly described below.

¹⁴To facilitate the discussion, in the notation for these quantities we shall distinguish, as it is customary (see e.g. [26]), the scale dependence described by the RG equations of continuum QCD (first argument) from the one due to $\mathcal{O}(a^2\tilde{p}^2)$ cutoff effects (second argument).

In order to reduce the statistical error, the lattice approximants of the Q_{VV+AA} RC have been averaged over an equivalent pattern of Wilson parameters (r_1, r_2, r_3, r_4) of valence quarks [namely, (1, 1, 1, -1) and (-1, -1, -1, 1)] as well as over different lattice momenta corresponding to the same value of \tilde{p}^2 . We have checked that performing these averages before or after taking the chiral limit leads to perfectly consistent (actually almost identical) results. The outcome of the whole analysis is conveniently expressed in terms of Z_{VA+AV}^{RGI} (M1) and Z_{VA+AV}^{RGI} (M2). These are the RGI quantities whose values are quoted in Table IV together with the values of the other RC's relevant for the B_K^{RGI} computation.

It is interesting to compare our results with those obtained from a one-loop perturbative lattice computation. For instance, in the case $\beta = 3.9$ one gets $Z_{VA+AV}^{1\text{-loop,RGI}} = 0.422$, if the perturbative gauge coupling is set to $g_0^2/\langle P \rangle$ ($\langle P \rangle$ is the plaquette expectation value), or $Z_{VA+AV}^{1\text{-loop,RGI}} = 0.675$, if the perturbative gauge coupling is set to the “boosted” value corresponding to the prescription of Ref. [40]. These numbers should be compared with the values in Table IV.

2. Valence chiral limit

For fixed values of β , $a^2\tilde{p}^2$, and $a\mu_{\text{sea}}$, we fit D_{11} [see Eq. (A7)] to the ansatz

$$D_{11}(p; \mu_{\text{val}}, \mu_{\text{sea}}) = A(\tilde{p}^2; \mu_{\text{sea}}) + B(\tilde{p}^2; \mu_{\text{sea}})\mu_{\text{val}} + C(\tilde{p}^2; \mu_{\text{sea}})(\mu_{\text{val}})^{-1}, \quad (\text{A9})$$

the form of which we would now like to justify.

In general, the RI-MOM approach relies on the fact that, at very large values of p^2 ($\gg \Lambda_{\text{QCD}}^2$), the relevant Green functions (and the associated vertices) are polynomial in all the quark mass parameters, because nonperturbative contributions which can violate this property vanish in this limit. However, at finite values of p^2 special care must be taken in studying the quark mass behavior of Green functions that admit one Goldstone boson (GB) intermediate state in their spectral decomposition. Indeed, such nonperturbative contributions to Green functions, though suppressed by a factor $1/p^2$ for each GB pole (see below), are divergent in the chiral limit and must hence be disentangled and removed. As explained in Appendix B of Ref. [41], this is precisely the case for the correlator G_{VV+AA} [see Eq. (A4)] and the associated vertex D_{11} .

By using the Lehmann-Symanzik-Zimmermann reduction formulas one finds that the GB-pole contributions relevant for (the spectral decomposition of) $D_{11}(p; \mu_{\text{val}}, \mu_{\text{sea}})$ are of the form¹⁵

¹⁵Here $q_1(p)$ denotes the four-dimensional Fourier transform of $q_1(x)$ with momentum p . As in Sec. II, M^{12} (M^{34}) is the mass of the lattice GB state $|P^{12}\rangle$ ($|P^{34}\rangle$).

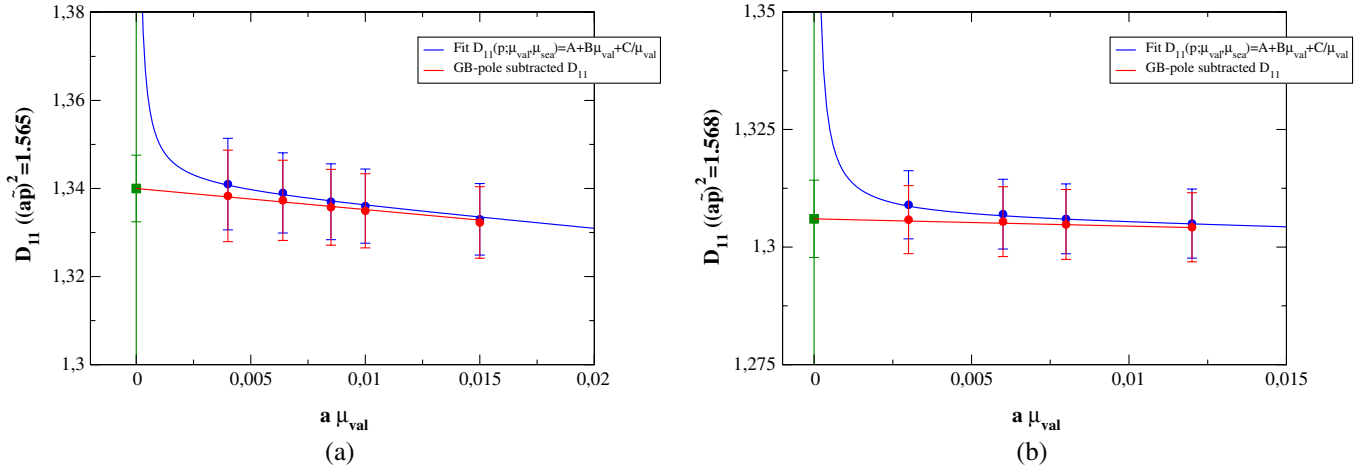


FIG. 8 (color online). GB-pole subtraction and valence chiral limit of D_{11} [see Eq. (A9)], plotted here vs $a\mu_{\text{val}}$, for $\beta = 3.9$, $a\mu_{\text{sea}} = 0.0040$, $a^2\tilde{p}^2 \approx 1.565$ (left panel) and $\beta = 4.05$, $a\mu_{\text{sea}} = 0.0030$, $a^2\tilde{p}^2 \approx 1.568$ (right panel).

- (i) $\frac{\Lambda_{\text{QCD}}^2}{(M^{34})^2 p^2} \langle P^{34} | Q_{VV+AA} q_1(p) \bar{q}_2(-p) | \Omega \rangle p^2$,
- (ii) $\frac{\Lambda_{\text{QCD}}^2}{(M^{12})^2 p^2} \langle \Omega | q_3(p) \bar{q}_4(-p) Q_{VV+AA} | P^{12} \rangle p^2$,
- (iii) $\frac{\Lambda_{\text{QCD}}^2}{(M^{34})^2 p^2} \langle P^{34} | Q_{VV+AA} | P^{12} \rangle \frac{\Lambda_{\text{QCD}}^2}{(M^{12})^2 p^2}$,

where, for simplicity, all the coefficients that are regular in the GB squared mass and weakly (at most logarithmically) dependent on p^2 have been set to unity. Furthermore, immaterial (for this discussion) lattice artifact corrections are neglected. As discussed in Sec. II, owing to the choice (2.4) of the valence quark Wilson parameters, the axial current $\bar{q}_4 \gamma_\mu \gamma_5 q_3$ is exactly conserved on the lattice (only broken by soft mass terms), while the conservation of $\bar{q}_2 \gamma_\mu \gamma_5 q_1$ is spoiled by lattice artifacts. From the form of Q_{VV+AA} it follows, in particular, that the matrix elements

$$\langle P^{34} | Q_{VV+AA} q_1(p) \bar{q}_2(-p) | \Omega \rangle, \quad \langle P^{34} | Q_{VV+AA} | P^{12} \rangle$$

vanish as $(M^{34})^2 \sim (\mu_3 + \mu_4)$ in the limit $\mu_{3,4} \rightarrow 0$. This property can be checked by using for these matrix elements the soft pion theorem associated with the conservation of the lattice current $\bar{q}_4 \gamma_\mu \gamma_5 q_3$ in order to reduce the GB particle P^{34} . Hence in the spectral decomposition of D_{11} no terms with two GB poles occur. Moreover, the terms (ii) and (iii) above, which both contain one GB pole, are strongly suppressed by factors of the kind a^2/p^2 and $(1/p^2)^2$, respectively.

In line with these arguments, a very smooth dependence of D_{11} on μ_{val} (or equivalently on M_{12}^2) is observed for all the momenta of interest in our analysis; see Fig. 8 for two typical examples. By fitting the D_{11} data to the ansatz (A9) the valence chiral limit is thus safely determined. A practically identical result is obtained by employing a fit ansatz analogous to (A9), with μ_{val} substituted by M_{12}^2 .

Combining the valence chiral limit lattice estimator of D_{11} with the corresponding approximant of Z_q (the valence chiral extrapolation of which poses no problems [26]) leads to reliable estimates of the intermediate quantities $Z_{VA+AV}^{\text{lat}}(\tilde{p}^2; a^2\tilde{p}^2; 0, a\mu_{\text{sea}})$.

3. Sea chiral limit

This limit is taken at fixed β and $a^2\tilde{p}^2$ by fitting the $Z_{VA+AV}^{\text{RI}}(\mu_0^2; a^2\tilde{p}^2; 0, a\mu_{\text{sea}})$ data to a polynomial of first order in $a^2\mu_{\text{sea}}^2$. Within our statistical errors (typically at the level of 1% to 2%) on the data at fixed $a\mu_{\text{sea}}$, the dependence on $a\mu_{\text{sea}}$ is hardly significant, as one can see e.g. from Fig. 9. We checked that repeating the whole analysis with $Z_{VA+AV}^{\text{RI}}(\mu_0^2; a^2\tilde{p}^2; 0, a\mu_{\text{sea}})$ fitted instead to a constant in $a\mu_{\text{sea}}$ leads to compatible results for the desired RC, but with smaller errors and often (but not

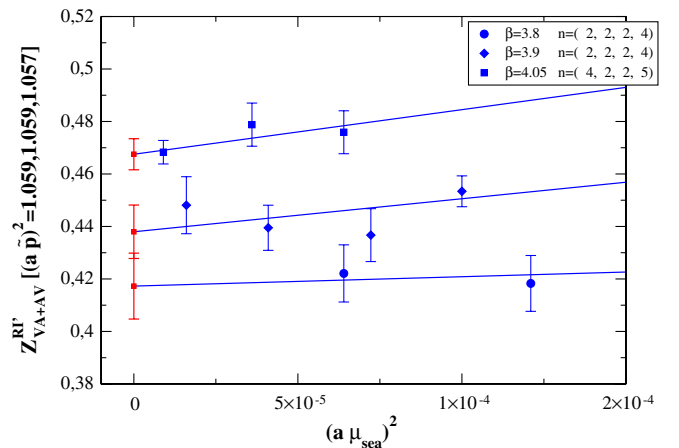


FIG. 9 (color online). The quantity $Z_{VA+AV}^{\text{RI}} \times (\tilde{p}^2; a^2\tilde{p}^2; 0, a\mu_{\text{sea}})$, taken at the valence chiral limit, as a function of $a^2\mu_{\text{sea}}^2$, for a typical lattice momentum choice (see inset) giving $a^2\tilde{p}^2 \sim 1.06$, for the three β values considered in this paper.

always, in particular, at $\beta = 3.9$ acceptable χ^2 values. Based on these findings we conservatively decided to perform the sea chiral extrapolation via a linear fit in $a^2\mu_{\text{sea}}^2$. In this way, we get the RC estimators $Z_{VA+AV}^{\text{RI}}(\mu_0^2; a^2\tilde{p}^2; 0, 0)$.

4. Removal of $O(a^2g^2)$ cutoff effects

Improved chiral limit RC estimators, $Z_{VA+AV}^{\text{RI-impr}}(\tilde{p}^2; a^2\tilde{p}^2)$, are obtained by removing from $Z_{VA+AV}^{\text{RI}}(\tilde{p}^2; a^2\tilde{p}^2; 0, 0)$ discretization errors up to $O(a^2g^2)$, viz.

$$\begin{aligned} Z_{VA+AV}^{\text{RI-impr}}(\tilde{p}^2; a^2\tilde{p}^2) &= Z_{VA+AV}^{\text{RI}}(\tilde{p}^2; a^2\tilde{p}^2; 0, 0) + \frac{g^2}{16\pi^2} a^2 \\ &\times \left[\tilde{p}^2 (c_{D_{11}}^{(1)} + c_{D_{11}}^{(2)} \log(a^2\tilde{p}^2)) + c_{D_{11}}^{(3)} \frac{\sum_{\rho} \tilde{p}_{\rho}^4}{\tilde{p}^2} \right] \\ &- \frac{g^2}{12\pi^2} 2a^2 \left[\tilde{p}^2 (c_q^{(1)} + c_q^{(2)} \log(a^2\tilde{p}^2)) + c_q^{(3)} \frac{\sum_{\rho} \tilde{p}_{\rho}^4}{\tilde{p}^2} \right]. \end{aligned} \quad (\text{A10})$$

The coefficients $c_q^{(j)}$, $j = 1, 2, 3$ can be found in Eq. (34) of Ref. [26], while the coefficients $c_{D_{11}}^{(j)}$, $j = 1, 2, 3$, namely,

$$\begin{aligned} c_{D_{11}}^{(1)} &= 2.64223, & c_{D_{11}}^{(2)} &= -19/18, \\ c_{D_{11}}^{(3)} &= -2.79899, \end{aligned} \quad (\text{A11})$$

have been recently computed by evaluating the vertex $D_{11}(p)$ [Eq. (A7)] in lattice perturbation theory to one-loop and including cutoff effects up to the second order in a [27]. Here we just recall that in lattice perturbation theory the vertex $D_{11}(p)$ can be expressed in the form

$$\begin{aligned} D_{11}(p)^{\text{pert}} &= 1 + \frac{g^2}{16\pi^2} [b_{D_{11}}^{(1)} + b_{D_{11}}^{(2)} \log(a^2\tilde{p}^2)] \\ &+ \frac{g^2}{16\pi^2} a^2 \left[\tilde{p}^2 (c_{D_{11}}^{(1)} + c_{D_{11}}^{(2)} \log(a^2\tilde{p}^2)) \right. \\ &\left. + c_{D_{11}}^{(3)} \frac{\sum_{\rho} \tilde{p}_{\rho}^4}{\tilde{p}^2} \right] + O(a^4g^2, g^4), \end{aligned} \quad (\text{A12})$$

and we refer to [27] for the values of the (here irrelevant) coefficients $b_{D_{11}}^{(1,2)}$ and all details. The form of Eq. (A10) follows directly from Eqs. (A6) and (A12) above, as well as from Eq. (32) of [26], where the perturbative expression of $\Sigma_1(p) = Z_q(p)$, including the $O(a^2g^2)$ corrections, is given.

In the numerical evaluation of the perturbative correction in Eq. (A10) g^2 was taken as the simple boosted coupling $\tilde{g}^2 \equiv g_0^2/\langle P \rangle$, where the average plaquette $\langle P \rangle$ is computed nonperturbatively. The values of $\langle P \rangle$ we employed here are [0.5689, 0.5825, 0.6014] for $\beta = [3.8, 3.9, 4.05]$, respectively. The (nice) effect of the (A10) correction in removing the unwanted $a^2\tilde{p}^2$ dependence is illustrated, in

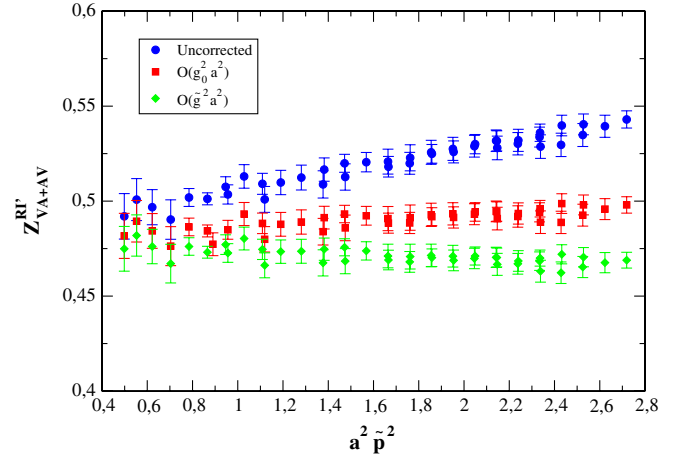


FIG. 10 (color online). The effect of subtracting from $Z_{VA+AV}^{\text{RI}}(\tilde{p}^2; a^2\tilde{p}^2; 0, 0)$ at $\beta = 4.05$ (blue dots) the $O(a^2g^2)$ correction (A10), setting either $g^2 = g_0^2$ (red squares) or $g^2 = \tilde{g}^2$ (green diamonds).

the case $\beta = 4.05$, in Fig. 10. In the figure the uncorrected values of $Z_{VA+AV}^{\text{RI}}(\tilde{p}^2; a^2\tilde{p}^2; 0, 0)$ are compared with the values of $Z_{VA+AV}^{\text{RI-impr}}(\tilde{p}^2; a^2\tilde{p}^2)$ obtained by setting either $g^2 = g_0^2 = 6/\beta$ or (as we chose in the end) $g^2 = \tilde{g}^2$.

5. Absence of wrong chirality mixings

According to the analysis of Ref. [14], at maximal twist wrong chirality mixings can affect the renormalization of Q_{VV+AA} only at order a^2 (or higher). The relation between the renormalized lattice and bare operators then has the form

$$\hat{Q}_{VV+AA}^{\text{RI}} = Z_{VA+AV}^{\text{RI}} \left[Q_{VV+AA} + \sum_{j=2}^5 \Delta_{1j} Q_j + \dots \right], \quad (\text{A13})$$

where (using the operator basis of Ref. [6]) we have

$$\begin{aligned} Q_2 &= 2\{[\bar{q}_1 \gamma_\mu q_2][\bar{q}_3 \gamma_\mu q_4] \\ &\quad - [\bar{q}_1 \gamma_\mu \gamma_5 q_2][\bar{q}_3 \gamma_\mu \gamma_5 q_4] + (q_2 \leftrightarrow q_4)\}, \\ Q_3 &= 2\{[\bar{q}_1 q_2][\bar{q}_3 q_4] - [\bar{q}_1 \gamma_5 q_2][\bar{q}_3 \gamma_5 q_4] + (q_2 \leftrightarrow q_4)\}, \\ Q_4 &= 2\{[\bar{q}_1 q_2][\bar{q}_3 q_4] + [\bar{q}_1 \gamma_5 q_2][\bar{q}_3 \gamma_5 q_4] + (q_2 \leftrightarrow q_4)\}, \\ Q_5 &= 2\{[\bar{q}_1 \sigma_{\mu\nu} q_2][\bar{q}_3 \sigma_{\mu\nu} q_4] + (q_2 \leftrightarrow q_4)\}. \end{aligned} \quad (\text{A14})$$

In Eq. (A13) the mixing coefficients Δ_{1j} are $O(a^2)$ quantities and “...” stands for higher order lattice corrections. In Fig. 11 we plot Δ_{1j} , $j = 2, 3, 4, 5$ as a function of $a^2\tilde{p}^2$ for $\beta = 3.8$, $\beta = 3.9$, and $\beta = 4.05$. It is clearly seen that in all cases the mixing coefficients are zero within errors and that this is systematically more so as β increases.

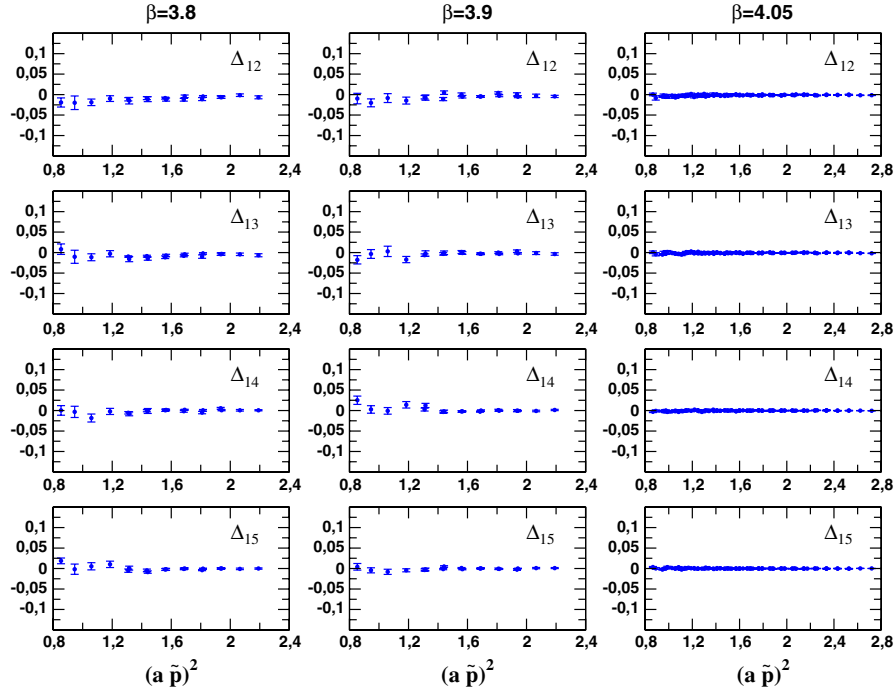


FIG. 11 (color online). The behavior of the mixing coefficients Δ_{1j} , $j = 2, 3, 4, 5$, as a function of $a^2 \tilde{p}^2$ for $\beta = 3.8$, $\beta = 3.9$, and $\beta = 4.05$, respectively.

6. Final estimates from M1 and M2 methods

The first step is to convert $Z_{VA+AV}^{RI'-impr}(\tilde{p}^2; a^2 \tilde{p}^2)$ to $Z_{VA+AV}^{RI'-impr}(\mu_0^2; a^2 \tilde{p}^2)$ by using the known formula for the NLO running [38,39]. This step is necessary in order to disentangle the $O(a^2 \tilde{p}^2)$ cutoff effects from the genuine continuum p^2 dependence, but the actual value of μ_0 has no impact on the RGI result for the RC. As customary, we take $\mu_0 = 1/a(\beta)$ for each value of β , namely, $1/a(3.8) = 2.0$ GeV, $1/a(3.9) = 2.3$ GeV, and $1/a(4.05) = 2.9$ GeV.

Method M1 consists in fitting $Z_{VA+AV}^{RI'-impr}(\mu_0^2; a^2 \tilde{p}^2)$ to the ansatz

$$Z_{VA+AV}^{RI'-impr}(\mu_0^2; a^2 \tilde{p}^2) = Z_{VA+AV}^{RI'}(\mu_0^2) + \lambda_{VA+AV} a^2 \tilde{p}^2 \quad (\text{A15})$$

in the large momentum region, $1.0 \leq a^2 \tilde{p}^2 \leq 2.2$. As expected, the slope λ_{VA+AV} exhibits a very mild gauge coupling dependence which (unlike the case of quark bilinear RC's) is not significant within our current statistical errors. We thus treat λ_{VA+AV} as a β -independent quantity. According to the ansatz (A15) a simultaneous linear extrapolation to $a^2 \tilde{p}^2 = 0$ at the three β values of interest was performed. The extrapolated values, $Z_{VA+AV}^{RI'}(\mu_0^2)$, are finally used to evaluate via Eq. (A1), to NLO accuracy, the quantities Z_{VA+AV}^{RGI} (M1) quoted in Table IV.

The numbers for $Z_{VA+AV}^{RI'-impr}(\mu_0^2; a^2 \tilde{p}^2)$ at the three β 's and the lines of the simultaneous best linear fit in $a^2 \tilde{p}^2$ are shown in Fig. 12. We recall that in this figure, as in all other figures presented in this appendix, only data points

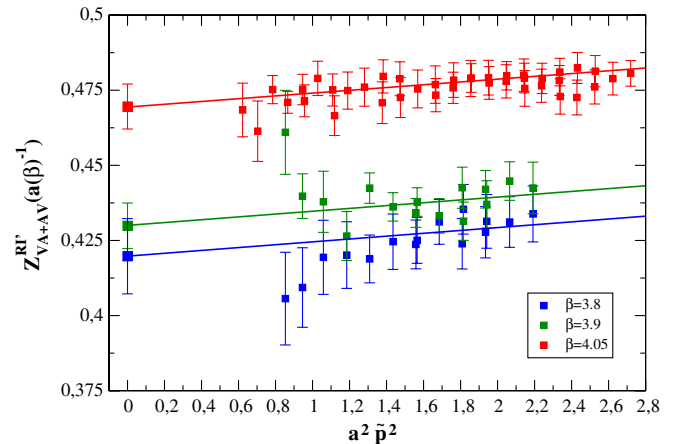


FIG. 12 (color online). $Z_{VA+AV}^{RI'-impr}(a(\beta)^{-2}; a^2 \tilde{p}^2)$ as a function of $a^2 \tilde{p}^2$ for the three β values considered in this paper. The three straight lines represent the simultaneous linear fit to the $Z_{VA+AV}^{RI'-impr}(a(\beta)^{-2}; a^2 \tilde{p}^2)$ data in the interval $1.0 \leq a^2 \tilde{p}^2 \leq 2.2$ at the three β 's.

corresponding to the momenta p satisfying the constraint (A8) appear. As we said above, data that refer to momenta p violating the condition (A8) are never used in our RC analysis.

When method M2 is used, we separately average at each β the values of $Z_{VA+AV}^{RI'-impr}(\mu_0^2; a^2 \tilde{p}^2)$ over a narrow interval of momenta where data are linear in $a^2 \tilde{p}^2$. In physical units we take the same momentum interval for all β 's, i.e. $\tilde{p}^2 \in [8.0, 9.5]$ GeV².

APPENDIX B: CHIRAL AND CONTINUUM EXTRAPOLATIONS

Here we give some details and discuss a few technical aspects of the auxiliary analyses that were performed, as discussed in Sec. III B 3, to estimate the systematic error on our B_K^{RGI} computation.

In order to evaluate the systematic errors affecting the extrapolation in the u/d -quark mass, which was performed together with that of the continuum limit, we also tried an analysis where the role of the renormalized quark masses, $\hat{\mu}_\ell$ and $\hat{\mu}_h$, is played by $(M_{\ell\ell}^{\text{tm}})^2$ and $(M_{hh}^{\text{tm}})^2$, i.e. the masses of the pseudoscalar mesons made out of two mass-degenerate quarks (regularized with opposite Wilson parameters, as implied by the label “tm”). The fit ansatz (3.1) was then replaced by the following one:

$$\begin{aligned} B_{K,\text{lat}}^{\text{RGI}}(M_{\ell\ell}^{\text{tm}}, M_{hh}^{\text{tm}}) &= B_{K,\chi}^{\text{RGI}}(M_{hh}^{\text{tm}}) \left[1 + b'(M_{hh}^{\text{tm}}) \frac{(M_{\ell\ell}^{\text{tm}})^2}{f_0^2} \right. \\ &\quad \left. - \frac{(M_{\ell\ell}^{\text{tm}})^2}{32\pi^2 f_0^2} \log \frac{(M_{\ell\ell}^{\text{tm}})^2}{16\pi^2 f_0^2} \right] + a^2 f_0^2 D'_B(M_{hh}^{\text{tm}}), \quad (\text{B1}) \end{aligned}$$

where $B_{K,\chi}^{\text{RGI}}(M_{hh}^{\text{tm}})$, $b'(M_{hh}^{\text{tm}})$, and $D'_B(M_{hh}^{\text{tm}})$ are the three fit parameters. For all values of β and $M_{\ell\ell}^{\text{tm}}$, data for $B_{K,\text{lat}}^{\text{RGI}}(M_{\ell\ell}^{\text{tm}}, M_{hh}^{\text{tm}})$ have first been interpolated in $(M_{hh}^{\text{tm}})^2$ in order to obtain the RGI bag parameter at three reference values of M_{hh}^{tm} , namely, $5.10f_0$, $5.50f_0$, $5.90f_0$. Then three continuum and chiral fits for $B_{K,\text{lat}}^{\text{RGI}}$ at these three reference values of M_{hh}^{tm} were performed, based on the ansatz (B1). The fits turned out to be of good quality and yielded continuum limit results for $B_K^{\text{RGI}}(M_\pi, M_{hh})$ at $M_\pi = 135$ MeV and $M_{hh} = (5.10, 5.50, 5.90)f_0$, respectively. For illustration, we report in Fig. 13 the results for the case of $M_{hh}^{\text{tm}} = 5.50f_0$. The extrapolated value $B_K^{\text{RGI}}(M_\pi, 5.50f_0)$ is represented by an open circle in the figure. As one can see from Fig. 14, the dependence of these extrapolated results on M_{hh}^2 is very mild and hardly significant compared to the 4% level of our statistical errors. In this situation the interpolation of $B_K^{\text{RGI}}(M_\pi, M_{hh})$ in $(M_{hh}^{\text{tm}})^2$ to the physical kaon mass [which we identified as the point where $(M_{hh}^{\text{tm}})^2 = 2M_K^2 - M_\pi^2$] poses no particular problem (see Fig. 14) and yields $B_K^{\text{RGI}} = 0.732(24)$. Notice that owing to the weak dependence of $B_K^{\text{RGI}}(M_\pi, M_{hh})$ on $(M_{hh}^{\text{tm}})^2$, the approximation induced by the use of the LO SU(3)- χ PT formula to relate $(M_{hh}^{\text{tm}})^2$ to the physical value of the $2M_K^2 - M_\pi^2$ mass difference turns out to have a completely negligible impact on the final result.

¹⁶The interpolation was based on global fits linear in $(M_{hh}^{\text{tm}})^2$. The fit quality was good in all cases, and the statistical error on the interpolation results has been estimated by a standard bootstrap procedure.

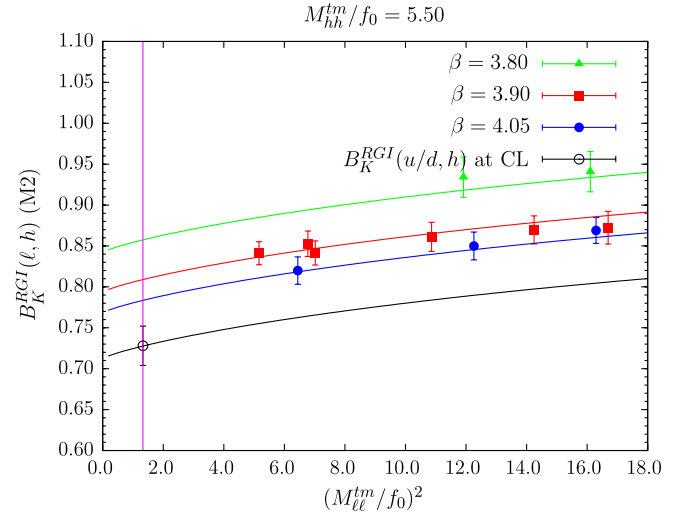


FIG. 13 (color online). Combined chiral and continuum fits according to the ansatz (B1) yielding B_K^{RGI} at $\hat{\mu}_h$, corresponding to $M_{hh}^{\text{tm}}/f_0 = 5.50$. The label M2 refers to the RI-MOM procedure adopted for the computation of Z_{VA+AV}^{RGI} and Z_A .

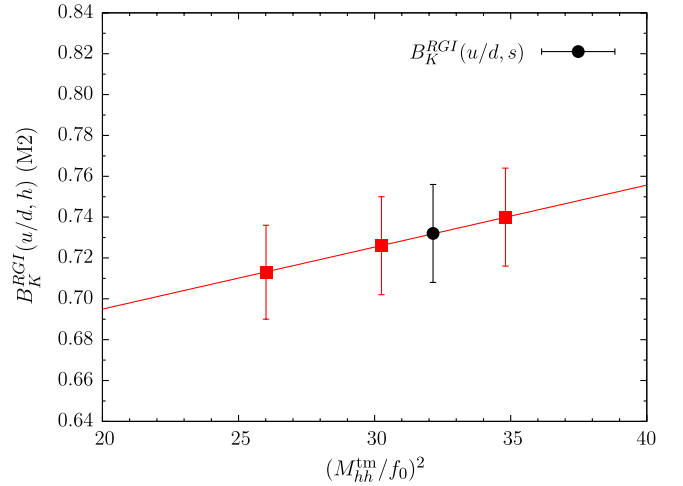


FIG. 14 (color online). B_K^{RGI} at the physical u/d -quark mass as a function of $(M_{hh}^{\text{tm}}/f_0)^2$. Squares represent the values computed as explained in the text at $M_{hh} = (5.10, 5.50, 5.90)f_0$. The interpolated value at the physical point $(M_{hh}^{\text{tm}})^2 = 2M_K^2 - M_\pi^2$ is indicated with a full dot. The label M2 has the same meaning as in Fig. 13.

With the purpose of estimating the systematic uncertainty due to the extrapolation of our B_K data to the pion (or u/d -quark) physical point, we also studied the effect of performing the chiral fit assuming a first or second order polynomial dependence on μ_ℓ [or $(M_{\ell\ell}^{\text{tm}})^2$]. The analysis of the $\hat{\mu}_h$ - and $\hat{\mu}_\ell$ -quark mass dependence, described in Sec. III B 2, was repeated with the chiral and continuum fit ansatz (3.1) replaced by

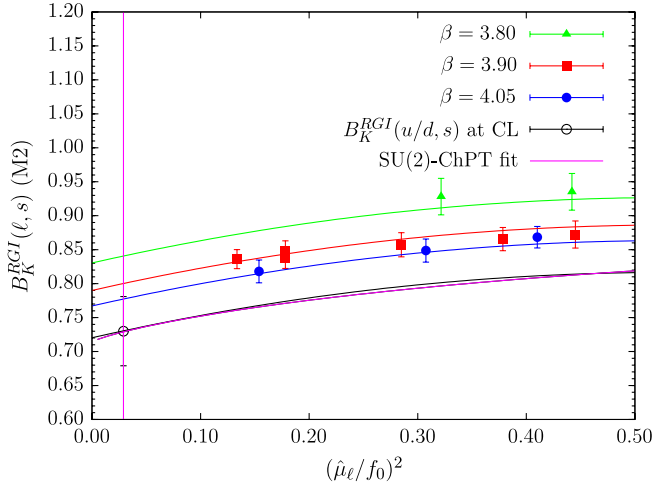


FIG. 15 (color online). Combined chiral and continuum fits B_K^{RGI} according to the ansatz (B2). The label M2 has the same meaning as in Fig. 13. For comparison, the continuum limit curve, corresponding to the ansatz (3.1) based on SU(2) χ Pt, is also shown.

$$B_{K,\text{lat}}^{\text{RGI}}(\hat{\mu}_\ell, \hat{\mu}_s) = B_{K,\chi}^{\text{RGI}}(\hat{\mu}_s) + C_1(\hat{\mu}_s) \frac{2\hat{B}_0 \hat{\mu}_\ell}{f_0^2} + C_2(\hat{\mu}_s) \left(\frac{2\hat{B}_0 \hat{\mu}_\ell}{f_0^2} \right)^2 + a^2 f_0^2 C_L(\hat{\mu}_s), \quad (\text{B2})$$

while always taking $\hat{\mu}_s = 92(5)$ MeV. In the case where only a linear dependence on $\hat{\mu}_\ell$ is assumed, we set $C_2(\hat{\mu}_s) \equiv 0$. Besides $B_{K,\chi}^{\text{RGI}}(\hat{\mu}_s)$, the other fit parameters in the formula (B2) are $C_L(\hat{\mu}_s)$, $C_1(\hat{\mu}_s)$, and (only for the case of a second order polynomial) $C_2(\hat{\mu}_s)$.

In the case of an assumed quadratic dependence of $B_{K,\text{lat}}^{\text{RGI}}$ data on $\hat{\mu}_\ell$, in the continuum limit and at the physical u/d -quark mass point, one finds $B_K^{\text{RGI}} = 0.730(51)$. The central value of this determination is perfectly in line with all our previous evaluations, only the associated statistical error is somewhat larger because here we have been dealing with a four (instead of a three) parameter fit. The good quality of the fit is well illustrated by Fig. 15. A good fit yielding $B_K^{\text{RGI}} = 0.750(26)$ is also obtained if just a simple linear dependence of the data on $\hat{\mu}_\ell$ is assumed. Not unexpectedly (given the distribution of data points) the central value of B_K^{RGI} in this case turns out to be slightly larger than in chiral fits that are based on SU(2) χ Pt or an ansatz allowing for some curvature in the $\hat{\mu}_\ell$ behavior. This effect, which is hardly larger than 1 (statistical) standard deviation, is taken into account in our systematic error budget (see Sec. III B 3).

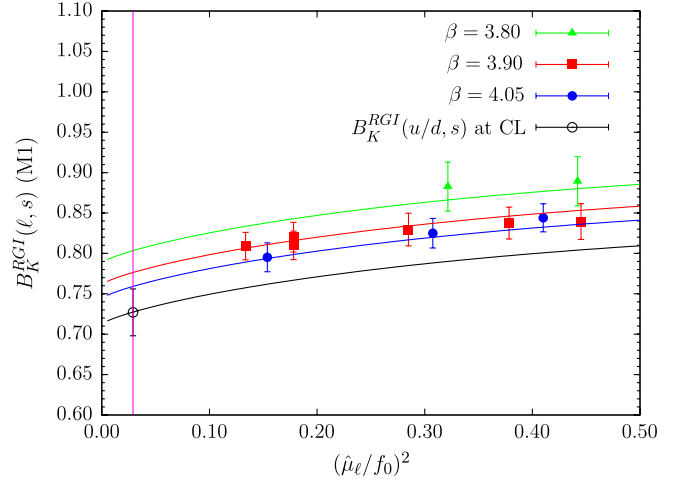


FIG. 16 (color online). Combined chiral and continuum fits of B_K^{RGI} according to the ansatz (3.1), for the case where the M1 method is adopted for the RI-MOM computation of both Z_{VA+AV}^{RGI} and Z_A —as implied by the label M1 in the ordinate.

For completeness we also show in Fig. 16 the chiral and continuum extrapolation of our B_K^{RGI} data when method M1 instead of M2 (see Ref. [26] and Appendix A) is employed in the RI-MOM computation of Z_A and Z_{VA+AV}^{RGI} . By an analysis otherwise identical to that discussed in Sec. III B 2, we obtain, in the continuum limit and at the physical pion mass point, $B_K^{\text{RGI}} = 0.727(30)$. As expected from the RC values reported in Table IV, in the present case the cutoff effects at finite lattice spacing are somewhat smaller, but the statistical errors are a bit larger compared to the case of Fig. 7.

As stated in Sec. III B 3, the effect of replacing with a/r_0 the scaling variable af_0 , to build dimensionless quantities in intermediate steps of our analyses and measure the distance from the continuum limit, is as small as 0.004–0.005. The curves illustrating our interpolation to the s -quark mass point and extrapolation to the u/d -quark point and continuum limit, in the case where a/r_0 is used as a scaling variable, look almost identical (within graphical resolution) to those we presented above and are hence not shown.

Other analyses were also performed corresponding to different variants of our reference analysis, discussed in Sec. III B 3. In all cases the values of B_K^{RGI} at the physical point were found to be very close to the value quoted in Eq. (3.6), with a spread that is well covered by our final estimate, ± 0.017 , of the systematic error.

- [1] A.J. Buras, *Weak Hamiltonian, CP Violation and Rare Decays*, edited by F. David and R. Gupta (Elsevier Science B.V., New York, 1997); [arXiv:hep-ph/0505175](#).
- [2] L. Lellouch, Proc. Sci., LAT2008 (2008) 015.
- [3] V. Lubicz, Proc. Sci., LAT2009 (2009) 013.
- [4] M. Bochicchio *et al.*, Nucl. Phys. **B262**, 331 (1985).
- [5] C.W. Bernard, T. Draper, G. Hockney, and A. Soni, Nucl. Phys. B, Proc. Suppl. **4**, 483 (1988).
- [6] A. Donini, V. Gimenez, G. Martinelli, M. Talevi, and A. Vladikas, Eur. Phys. J. C **10**, 121 (1999).
- [7] D. Becirevic *et al.*, Phys. Lett. B **487**, 74 (2000).
- [8] D. Becirevic *et al.*, Eur. Phys. J. C **37**, 315 (2004).
- [9] P. Dimopoulos, J. Heitger, F. Palombi *et al.* (ALPHA Collaboration), Nucl. Phys. **B776**, 258 (2007).
- [10] P. Dimopoulos *et al.* (ALPHA Collaboration), Nucl. Phys. **B749**, 69 (2006).
- [11] R. Frezzotti, P.A. Grassi, S. Sint, and P. Weisz (ALPHA Collaboration), J. High Energy Phys. **08** (2001) 058.
- [12] R. Frezzotti and G.C. Rossi, J. High Energy Phys. **08** (2004) 007.
- [13] C. Pena, S. Sint, and A. Vladikas (ALPHA Collaboration), J. High Energy Phys. **09** (2004) 069.
- [14] R. Frezzotti and G.C. Rossi, J. High Energy Phys. **10** (2004) 070.
- [15] P. Dimopoulos, H. Simma, and A. Vladikas (ALPHA Collaboration), J. High Energy Phys. **07** (2009) 007.
- [16] R. Frezzotti and G. Rossi, Proc. Sci., LAT2007 (2007) 277.
- [17] P. Dimopoulos, R. Frezzotti, C. Michael, G.C. Rossi, and C. Urbach (ETM Collaboration), Phys. Rev. D **81**, 034509 (2010).
- [18] G. Martinelli, C. Pittori, C.T. Sachrajda, M. Testa, and A. Vladikas, Nucl. Phys. **B445**, 81 (1995).
- [19] P. Dimopoulos *et al.* (ETM Collaboration), Proc. Sci., LATTICE2008 (2008) 271.
- [20] V. Bertone *et al.* (ETM Collaboration), Proc. Sci., LAT2009 (2009) 258.
- [21] P. Weisz, Nucl. Phys. **B212**, 1 (1983).
- [22] P. Boucaud *et al.* (ETM Collaboration), Phys. Lett. B **650**, 304 (2007).
- [23] K. Osterwalder and E. Seiler, Ann. Phys. (N.Y.) **110**, 440 (1978).
- [24] R. Frezzotti, G. Martinelli, M. Papinutto, and G.C. Rossi, J. High Energy Phys. **04** (2006) 038.
- [25] R. Baron *et al.* (ETM Collaboration), J. High Energy Phys. **08** (2010) 097.
- [26] M. Constantinou *et al.* (ETM Collaboration), J. High Energy Phys. **08** (2010) 068.
- [27] M. Constantinou, V. Lubicz, H. Panagopoulos, and F. Stylianou, J. High Energy Phys. **10** (2009) 064; M. Constantinou, P. Dimopoulos, R. Frezzotti, V. Lubicz, H. Panagopoulos, A. Skouroupathis, and F. Stylianou, [arXiv:1011.6059](#).
- [28] P. Boucaud *et al.* (ETM Collaboration), Comput. Phys. Commun. **179**, 695 (2008).
- [29] C. Aubin, J. Laiho, and R.S. Van de Water, Phys. Rev. D **81**, 014507 (2010).
- [30] C. Allton *et al.* (RBC-UKQCD Collaboration), Phys. Rev. D **78**, 114509 (2008).
- [31] G. Colangelo, S. Durr, and C. Haefeli, Nucl. Phys. **B721**, 136 (2005).
- [32] B. Blossier *et al.* (ETM Collaboration), Proc. Sci., LAT2010 (2010) 179 [[arXiv:1011.1862](#)].
- [33] A.J. Buras and D. Guadagnoli, Phys. Rev. D **78**, 033005 (2008).
- [34] R.S. Van de Water, Proc. Sci., LAT2009 (2009) 014 [[arXiv:0911.3127](#)].
- [35] M. Bona *et al.*, Proc. Sci., EPS-HEP2009 (2009) 160.
- [36] A.J. Buras, D. Guadagnoli, and G. Isidori, Phys. Lett. B **688**, 309 (2010).
- [37] R. Baron *et al.* (ETM Collaboration), J. High Energy Phys. **06** (2010) 111.
- [38] M. Ciuchini, E. Franco, V. Lubicz, G. Martinelli, I. Scimemi, and L. Silvestrini, Nucl. Phys. **B523**, 501 (1998).
- [39] A.J. Buras, M. Misiak, and J. Urban, Nucl. Phys. **B586**, 397 (2000).
- [40] S. Aoki *et al.* (JLQCD Collaboration), Phys. Rev. D **68**, 054502 (2003).
- [41] D. Becirevic, V. Gimenez, V. Lubicz, G. Martinelli, M. Papinutto, and J. Reyes, J. High Energy Phys. **08** (2004) 022.
- [42] Y. Aoki *et al.*, Phys. Rev. D **73**, 094507 (2006).
- [43] Y. Nakamura, S. Aoki, Y. Taniguchi, and T. Yoshie (CP-PACS Collaboration), Phys. Rev. D **78**, 034502 (2008).
- [44] Y. Aoki *et al.*, Phys. Rev. D **72**, 114505 (2005).
- [45] S. Aoki *et al.* (JLQCD Collaboration), Phys. Rev. D **77**, 094503 (2008).
- [46] C. Kelly, P.A. Boyle, and C.T. Sachrajda (RBC Collaboration and UKQCD Collaboration), Proc. Sci., LAT2009 (2009) 087.
- [47] T. Bae *et al.*, [arXiv:1008.5179](#) [Phys. Rev. D (to be published)].